

# Reaction Environment Impacts Charge Transfer But Not Chemical Reaction Steps in Hydrogen Evolution Catalysis

Bryan Y. Tang, Ryan P. Bisbey, Kunal M. Lodaya, Wei Lun Toh, Yogesh Surendranath\*

Department of Chemistry, Massachusetts Institute of Technology, Cambridge, Massachusetts 02139, United States

**Abstract:** Electrocatalysis occurring at an electrode interface involves elementary chemical and charge transfer reaction steps, with the kinetics of each step contributing to the overpotential requirement at a given reaction rate. Typical experiments report on the aggregate rate-overpotential profile with no information about the relative contributions from charge transfer and chemical steps. For the hydrogen evolution reaction (HER), the applied overpotential can be partitioned into a charge transfer overpotential, the overpotential necessary to drive proton-coupled electron transfer (PCET) to and from the surface, and a chemical overpotential, corresponding to a change in surface H activity. Reaction conditions can affect either or both the charge transfer and chemical components. Herein, we employ a Pd membrane double cell to spatially separate the charge transfer and chemical reactions steps of HER catalysis, enabling quantification of the chemical and charge transfer overpotential. We further analyze how each depend on pH, and the introduction of HER poisons and promoters. We find that for a given rate of H<sub>2</sub> release, the chemical overpotential is constant across diverse reaction environments whereas the charge transfer overpotential is strongly sensitive to reaction conditions. These findings suggest that reaction condition dependent-HER efficiencies are driven predominantly by changes to the kinetics of charge transfer rather than the chemical reactivity of surface H.

The interconversion of electrical and chemical energy requires catalysts that can mediate complex multi-electron, multi-proton reactions. When the electrocatalyst itself is the electrode, it facilitates these complex reactions by binding and stabilizing surface intermediates.<sup>1,2</sup> Thus, an overall electrocatalytic mechanism invariably consists of a sequence of elementary reaction steps that can be broadly bifurcated as either charge transfer steps (those involving the transit of ions across the electrical double layer to form surface bound intermediates) or chemical reaction steps (those involving the reaction of those surface intermediates with each other).<sup>3,4</sup> The rational design of improved electrocatalysts requires a detailed understanding of the relative contributions from charge transfer and chemical reaction kinetics to the overall reaction efficiency and how each depend on key reaction variables such as electrolyte, pH, and potential.

The thermochemistry and kinetics of both the charge transfer and chemical reaction steps are affected by the applied potential. This underappreciated concept can be understood in the context of the hydrogen evolution reaction (HER). In one viable mechanism for the HER (the Volmer-Tafel mechanism), the key surface H intermediate, historically termed overpotential deposited H (H<sub>OPD</sub>), is formed through charge transfer of a proton across the electrical double layer, followed by a chemical reaction step wherein two H<sub>OPD</sub> species recombine to form H<sub>2</sub> (Fig. 1).<sup>5,6</sup> For this mechanism, changes to the applied potential serve to directly increase the driving force and rate of the charge transfer step. This higher rate of H<sub>OPD</sub> formation must be balanced by an equally higher rate of H<sub>OPD</sub> recombination to form H<sub>2</sub> at steady state. Thus, the H<sub>OPD</sub> surface coverage will increase until the rate of H<sub>OPD</sub> formation via charge transfer and consumption via recombination are matched.<sup>7-9</sup> This indirect change in the H<sub>OPD</sub> coverage and corresponding activity (a<sub>H</sub>) can be viewed as a “chemical overpotential”,  $\eta_{\text{chemical}}$  (Fig. 1a, blue), which we define as the change in the chemical potential of surface H ( $\mu_H$ ) relative to its value in equilibrium with 1 atm H<sub>2</sub> ( $\mu_{H,0}$ , defined as  $\mu_H$  at the reversible hydrogen electrode potential) such that:

$$\eta_{\text{chemical}} = \frac{\mu_H - \mu_{H,0}}{F} = \frac{RT}{F} \ln \frac{a_H}{a_{H,0}}$$

where  $a_{H,0}$  is the chemical activity of surface H at the reversible hydrogen electrode potential in the presence of 1 atm of H<sub>2</sub> (see SI for derivation),  $F$  is Faraday's constant, and  $R$  is the gas constant and  $T$  is temperature.

Within this framework, the overall overpotential for HER catalysis partitions into a fraction going towards accelerating the rate of the charge transfer step to form H<sub>OPD</sub>. We define this as the charge transfer overpotential,  $\eta_{\text{charge transfer}}$  (Fig. 1a, red). The remainder goes towards accelerating the rate of the chemical reaction step for forming H<sub>2</sub>, (chemical overpotential,  $\eta_{\text{chemical}}$ ).<sup>7</sup> Although the foregoing logic emphasizes, qualitatively, that both  $\eta_{\text{charge transfer}}$  and  $\eta_{\text{chemical}}$  vary with the applied potential; the quantitative partitioning between the two is unknown. This is because a

typical polarization experiment only reports on the aggregate current-overpotential profile, and, thus, contains no information about the *individual* overpotential contributions that affect the charge transfer and chemical steps.

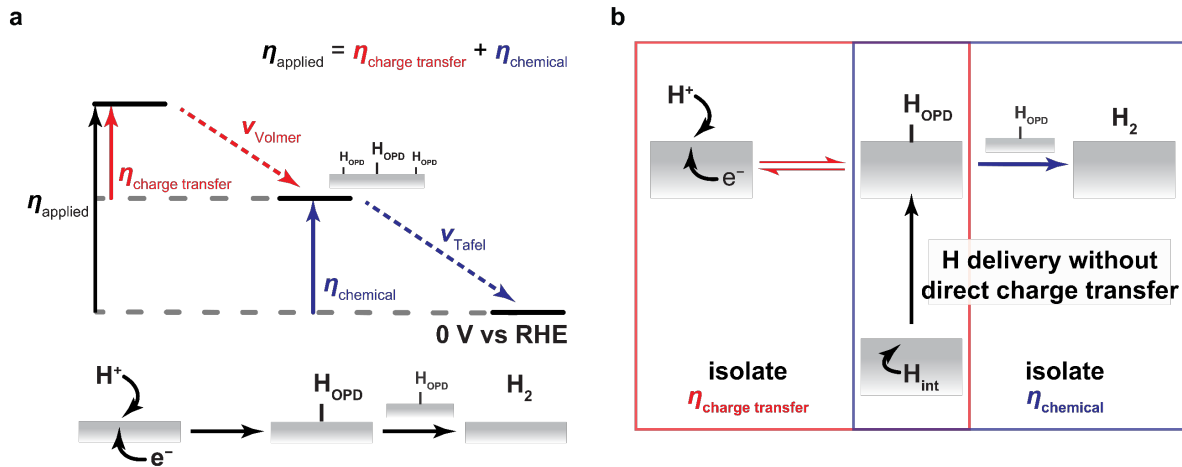


**Fig. 1 | Overpotential in hydrogen electrocatalysis on electrode interfaces is comprised of both chemical and charge transfer overpotential components.** **a**, Free energy schematic for the electrochemical hydrogen evolution reaction, with overpotential deposited H, H<sub>OPD</sub>, as the key surface intermediate for the reaction. Under polarization, the applied overpotential ( $\eta_{\text{applied}}$ ), is the aggregate of two overpotential components, the charge transfer overpotential ( $\eta_{\text{charge transfer}}$ ), and the chemical overpotential ( $\eta_{\text{chemical}}$ ). **b**, Diagrammatic representation of how using interstitial H (H<sub>int</sub>) delivery through a Pd membrane, decouples the  $\eta_{\text{charge transfer}}$  and  $\eta_{\text{chemical}}$  interdependencies for H<sub>OPD</sub> formation and H<sub>2</sub> evolution.

It is now widely appreciated that the overall kinetics of HER are strongly dependent on reaction conditions: on noble metals, HER kinetics are attenuated by two orders of magnitude in base vs acid;<sup>10–15</sup> the presence of alkali cations and buffering anions in the electrolyte can promote HER kinetics;<sup>16–19</sup> and surface bound species are known to both promote<sup>13,20,21</sup> and inhibit<sup>22–24</sup> catalysis. In all these cases, it remains unclear whether these dramatic effects stem from changes in the thermokinetic profile of the charge transfer steps, the chemical reaction steps, or some combination of both. Yet, a detailed understanding of the factors which control the reaction condition-dependence of the HER is a prerequisite for the rational design of improved catalysts and systems that operate under a wide array of reaction conditions.

Unfortunately, there currently exist a paucity of methods for discriminating the chemical and charge transfer contributions to overall HER catalytic efficiency and correspondingly their reaction condition-dependence. This stems directly from the difficulty in quantifying the population, much less the chemical activity or reaction condition-dependence of H<sub>OPD</sub> in the catalytic cycle. As the key reactive H intermediates for the HER, H<sub>OPD</sub> species exist at a thermodynamic excess relative to H<sub>2</sub> and are thus constantly being consumed under reaction conditions to release H<sub>2</sub>. Although the precise chemical bonding environment remains contentious,<sup>25</sup> H<sub>OPD</sub> stands in stark contrast to strongly bound, under-potential deposited H, H<sub>UPD</sub>, which form at potentials positive of the H<sup>+</sup>/H<sub>2</sub> equilibrium potential, are persistent on noble metal surfaces, and have been the subject of extensive thermodynamic and kinetic studies.<sup>11,13</sup> Spectroscopic studies have been able to observe and quantify H<sub>OPD</sub> population on Pt surfaces under steady state catalysis conditions, but correlating the surface population of H<sub>OPD</sub> with its chemical potential remains elusive.<sup>26,27</sup> Electrochemical transient methods have also been applied to quantify the activity of H<sub>OPD</sub> on a variety of metals.<sup>3,28–31</sup> While valuable, this technique, which tracks the decay of the open circuit potential following catalysis, inherently conflates double layer and adsorption contributions to electrode capacitance, making it hard to extract the H<sub>OPD</sub> population or energetics unequivocally. This problem is compounded when comparing data across vastly different reaction conditions where additional contributions to capacitance cannot be excluded. Thus, improved strategies for quantifying the thermodynamics and kinetics of highly reactive H<sub>OPD</sub> are needed to discriminate the relative contributions to medium-dependent HER kinetics.

The above challenges could be addressed if the critical H<sub>OPD</sub> intermediates could be generated and delivered in a tuneable fashion to the catalyst surface from an external source rather than via charge transfer to the H<sub>2</sub> evolving interface. We postulated that independent control of the surface population of H<sub>OPD</sub> would allow us to unambiguously generate a chemical overpotential without the need for charge transfer to the interface. This external delivery of H<sub>OPD</sub>

cannot be achieved on all noble metals; however, Pd is capable of intercalating H species which can diffuse rapidly within the bulk of the metal.<sup>32,33</sup> This property has been used to facilitate H<sub>2</sub> separations through thin Pd membranes.<sup>33–35</sup> Additionally, electrochemical polarization of a thin Pd membrane has been used to drive H transport to a second medium to carry out hydrogenation reactions.<sup>36–43</sup> Thus, we envisioned that H transport through a Pd membrane (**Fig. 1b**) could be employed to externally control the surface population of H<sub>OPD</sub> without charge transfer to the interface and uncover how different reaction conditions affect the chemical and charge transfer overpotential contributions to HER catalysis.

Herein, we employ electrochemically driven H-insertion at one face (the H-pumping interface) of a thin Pd membrane to establish a tuneable, controlled H<sub>OPD</sub> chemical potential at the opposite face (the analytical interface). We find, through a series of mechanistic studies, that the open circuit potential of the analytical interface directly measures the chemical overpotential for H<sub>2</sub> evolution. We vary the rate of H-insertion to the analytical interface and correlate the shift in the open circuit potential of the analytical interface with the rate of H<sub>2</sub> evolution at that interface to isolate the  $\eta_{\text{chemical-rate}}$  scaling for H<sub>2</sub> evolution catalysis (**Fig. 1b**, blue box). We further compare this scaling across a range of pH values, and in the presence of poisoning CO, and promoting Ni(OH)<sub>2</sub>. Remarkably, these studies reveal that across all the reaction conditions examined, the  $\eta_{\text{chemical-rate}}$  correlation plots overlay with a common scale factor of  $\sim 20$  mV dec<sup>-1</sup>. The data indicate that, upon normalizing to an equivalent  $\eta_{\text{chemical}}$ , the rate of net H-H recombination is remarkably insensitive to pH, or the presence of promoters or poisons. By super-imposing a small additional electrical polarization at the analytical interface on top of a high and fixed rate of H-insertion from the sub-surface, we isolate the rate-overpotential scaling for the charge transfer step of HER at a nominally fixed H<sub>OPD</sub> population (**Fig. 1b**, red box). Unlike the chemical overpotential, we find that the  $\eta_{\text{charge transfer-rate}}$  scaling for the HER is dramatically impacted by electrolyte pH and the presence of promoters or poisons. Thus, we conclude that the reaction condition dependence of the HER on Pd catalysts results predominantly from the promotion or inhibition of the charge transfer kinetics between Pd and the electrolyte, rather than changes in the intrinsic rate of the chemical reaction steps involving surface H. Taken together, these findings reveal the importance of considering both the chemical and charge transfer contributions to HER overpotential, and how changing reaction conditions modulate these two components independently to define the overall reaction efficiency.

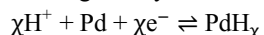
## RESULTS AND DISCUSSION

### Electrochemical Double Cell Enables Quantification of the Chemical Overpotential for Hydrogen Catalysis.

*Pd Membrane Electrochemical Double Cell Generates H<sub>OPD</sub> Without Direct Charge Transfer to that Interface.*

In order to discriminate the chemical and charge transfer contributions to HER activity, we constructed a Pd membrane electrochemical double cell (**Fig. 2**, see SI for full experimental details).<sup>44</sup> This configuration, which is also historically known as a Devanathan-Stachurski cell,<sup>32</sup> consists of two distinct electrochemical cells separated by a Pd foil, which serves as the working electrode for both electrochemical cells with separate counter and reference electrodes in each. Importantly, the pin-hole free nature of the Pd working electrode restricts the permeation of any liquids or electrolyte from one side to the other, thereby ionically isolating the two electrochemical cells.<sup>42</sup> Consequently, in this configuration, even though the working electrode is a single piece of metal and is contacted by two potentiostats, the current path for each electrochemical cell is distinct and, thus, no current flows from one face of the metal to the other. Consequently, each face of the common metal membrane can be independently polarized via charge transfer from the external circuit for that particular cell.

Most noble metal foils are completely impervious and thus polarization of one face has no effect on the other. However, Pd can form bulk PdH <sub>$\chi$</sub>  under reductive polarization in aqueous electrolytes, with the H fraction,  $\chi$ , driven to higher values upon increased negative polarization as given by the following electrochemical equilibrium:<sup>32,42</sup>



Consequently, polarization of one Pd interface, termed the H-pumping interface, in an electrochemical double cell generates H<sub>OPD</sub> species competent for H<sub>2</sub> release on the other, termed the analytical interface. Independently, the potential of the analytical interface of the Pd membrane can be measured and/or polarized by a second potentiostat, allowing us to probe the reactivity of H<sub>OPD</sub> species in HER catalysis at the analytical interface at a steady state population that has been orthogonally generated without net charge transfer at the analytical interface.

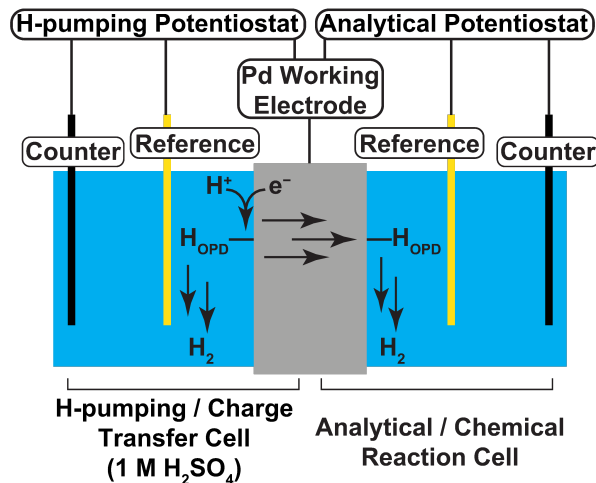


**Fig. 2 | Illustration of the electrochemical double cell configuration.** The electrochemical double cell consists of two electrochemical cells that are ionically isolated from one another despite sharing a common working electrode. In this electrochemical double cell configuration, proton reduction at the H-pumping interface generates  $H_{OPD}$ . The  $H_{OPD}$  at the H-pumping interface can then either spontaneously generate  $H_2$  at the H-pumping interface, or diffuse into Pd and reform  $H_{OPD}$  at the analytical interface, where it is competent for  $H_2$  release. Notably, charge transfer involved in  $H_{OPD}$  formation is isolated at the H-pumping interface, and is absent at the  $H_2$  evolving analytical interface.

Using the above electrochemical double-cell configuration, we tracked the open circuit potential (OCP) of the analytical interface upon polarizing the H-pumping interface. For this initial investigation, the electrolyte in the analytical cell was identical to the 1 M  $H_2SO_4$  electrolyte in the H-pumping cell, and the analytical cell was kept under 1 atm of  $H_2$ . At a  $-1\text{ mA cm}^{-2}$  current density applied to the H-pumping interface, we observe a steady state OCP at the analytical interface of  $-12\text{ mV}$  versus the reversible hydrogen electrode (RHE). This OCP value at the analytical interface shifts negatively in a linear fashion as the current passed at the H-pumping interface is increased logarithmically, reaching  $-47\text{ mV}$  vs RHE at a current density of  $-100\text{ mA cm}^{-2}$  at the H-pumping interface (Fig. 3a, red). Consistent with the OCP value being well-negative of RHE, we observe vigorous  $H_2$  evolution at the analytical interface (see below for quantitative analysis of  $H_2$  release kinetics). The analytical interface also exhibits no history effects, reaching the same steady state OCP value at a given current passed at the H-pumping interface irrespective of previous degrees of polarization at that interface. A linear fit to the data in Fig. 3a returns a slope of  $-17\text{ mV}$  change in OCP at the analytical interface per decade increase in current passed at the H-pumping interface. Upon termination of the polarization at the H-pumping interface (Fig. 3b, blue region), the OCP value decays towards more positive potentials as continued  $H_2$  release lowers the interstitial and surface H populations, with analogous behaviour observed at the H-pumping interface (Fig. S7). Importantly, when the Pd working electrode is replaced with a Pt foil, which does not intercalate or transport H, the OCP at the analytical interface is invariant with the amount of current passed and corresponding polarization at the opposite face of the Pt foil (Fig. 3a, black). Thus, under 1 atm  $H_2$ , the Pt analytical interface remains pinned to the RHE irrespective of the current passed at the H-pumping interface. The foregoing data establishes that increased reductive electrochemical polarization of the H-pumping interface leads a systematic and progressive change in the open circuit electrochemical potential of the analytical interface as a direct result of H-transport through the Pd membrane.

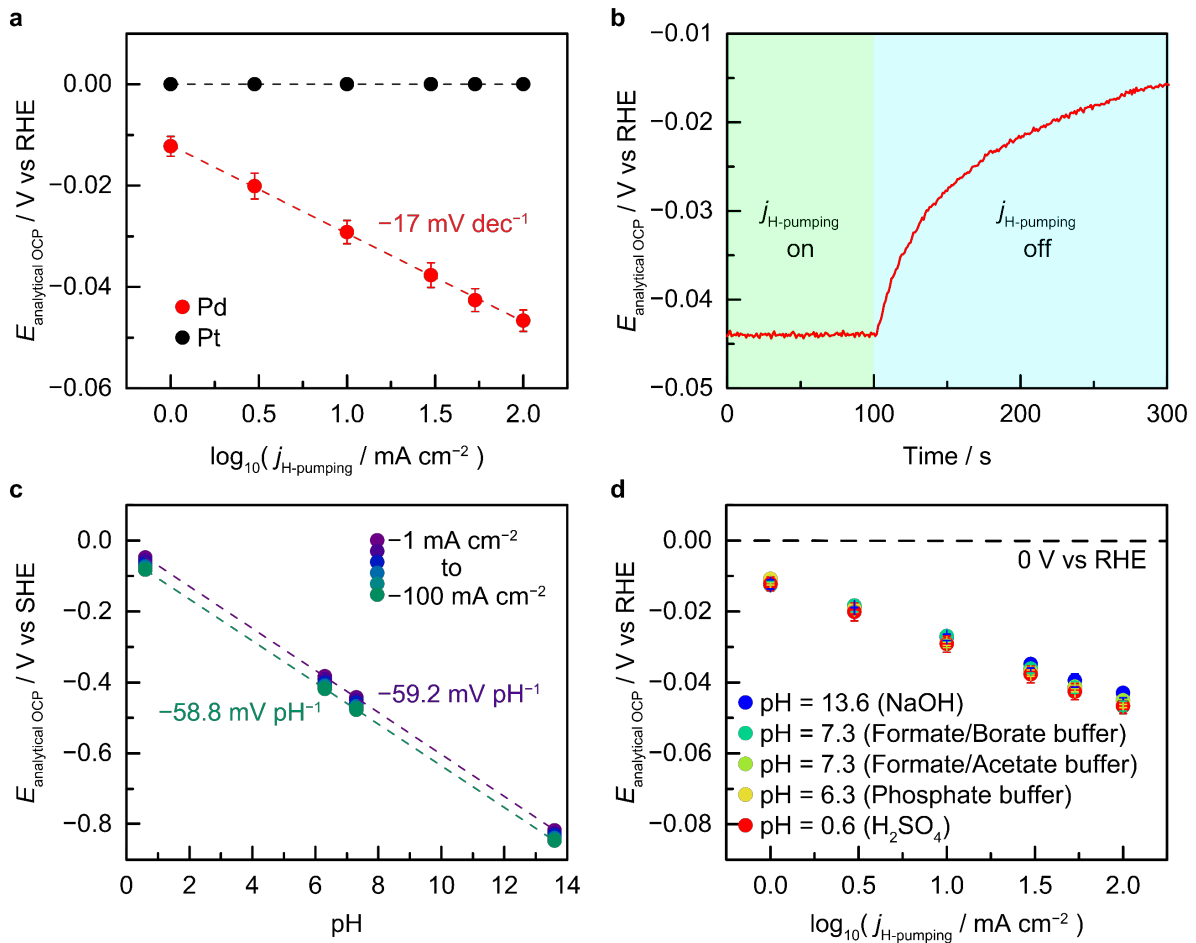


**Fig. 3 | Polarization of the H-pumping interface affects the OCP behaviour of the analytical interface.** **a**, OCP dependence of the analytical interface ( $E_{\text{analytical OCP}}$ ) under Galvanostatic polarization at the H-pumping interface ( $j_{\text{H-pumping}}$ ) in a symmetric double cell configuration (1 M  $\text{H}_2\text{SO}_4$  on both compartments), with Pd (red) and Pt (black) working electrodes. **b**, OCP of the analytical interface (red) under Galvanostatic polarization of  $-100 \text{ mA cm}^{-2}$  at the H-pumping interface ( $j_{\text{H-pumping}}$  on, green region) and immediately after polarization is turned off ( $j_{\text{H-pumping}}$  off, blue region). **c**, pH dependence of the analytical interface OCP vs the pH independent SHE potential ( $E_{\text{analytical OCP}}$ ) under Galvanostatic polarizations ranging from  $-1$  to  $-100 \text{ mA cm}^{-2}$  at the H-pumping interface (error bars are smaller than the data point markers). **d**, OCP dependence of the analytical interface vs the pH-dependent RHE potential ( $E_{\text{analytical OCP}}$ ) under Galvanostatic polarization at the H-pumping interface ( $j_{\text{H-pumping}}$ ) under different electrolyte pH conditions including 13.6 (blue), 7.3 (green), 7.3 (yellow), 6.3 (yellow) and 0.6 (red) (some error bars are smaller than the data point markers). Error bars indicate standard deviations obtained from three or more independent replicates.

#### *The Potential of the Analytical Interface Scales Nernstianly with Electrolyte pH.*

In order to determine the impact of the electrolyte pH on the OCP of the analytical interface, we set up an asymmetric electrochemical double cell. This asymmetric cell retained the same 1 M  $\text{H}_2\text{SO}_4$  electrolyte in the H-pumping cell, but we systematically varied the pH and composition of the electrolyte in the analytical cell. This approach fixes a common reaction environment for generating reactive H species in the H-pumping cell, but allows us to probe  $\text{H}_2$  evolution across a range of electrolyte conditions in the analytical cell. Importantly, the composition of electrolyte only perturbs the interface between electrode and electrolyte, and should have no influence on the transport of reactive H species through the Pd membrane, which is a bulk property of the electrode. We stress that this orthogonalization is impossible to achieve in a typical electrochemical HER experiment at a single interface. We tracked the OCP of the analytical interface across a range of pH values, and find that the potential of the analytical interface shifts by 59 mV per pH unit (Fig. 3c). This slope is preserved across a range of current densities, ranging of  $-1$  to  $-100 \text{ mA cm}^{-2}$ , passed at the H-pumping interface (Fig. 3c, purple to green). This Nernstian scaling with pH is also shown in Fig. 3d, where, across two orders of magnitude of current passed at the H-pumping interface, the OCP at the analytical interface remains largely unchanged versus the RHE reference (which by definition scales by  $59 \text{ mV pH}^{-1}$ ). Additionally, the data in Fig. 3d highlights that

across all pH conditions, the OCP measured at the analytical interface is driven well negative of the reversible hydrogen potential and that the  $-17$  mV slope observed for the symmetrical double cell above is also preserved across the entire pH range. Furthermore, at circumneutral pH, the OCP at the analytical interface is independent of the buffer composition, with identical values recorded for formate/borate, formate/acetate, and phosphate buffers (**Fig. 3d, greens**). Together the data evince that the electrochemical potential of the analytical interface scales in a purely Nernstian fashion with pH and is otherwise insensitive to the electrolyte composition.

*The Open Circuit Potential at the Analytical Interface Isolates the Chemical Overpotential for  $H_2$  evolution.*

The above findings provide insight into the reactions that determine the potential of the analytical interface during steady state H-pumping. Since the OCP is the potential at which zero net current passes, it reflects the potential at which the aggregate rate of anodic and cathodic charge transfer processes are balanced at the analytical interface. Thus, the foregoing data provide insight into the chemical participants in the charge transfer processes that set the OCP at the analytical interface. First, logarithmically increasing the current passed at the H-pumping interface leads to a linear shift of the analytical OCP on Pd to more negative values, an observation that is not retained on Pt (**Fig. 3a**). This implies that the interstitial H species, which are driven to higher fractions at higher H-pumping currents, are necessary for the induced spontaneous polarization of the analytical interface with the passage of reductive current at the H-pumping interface. Second, the strong Nernstian pH dependence (**Fig. 3c and 3d**) of the OCP indicates that the OCP is sampling a proton-coupled electron transfer (PCET) process involving an equal number of electrons and protons. Third, the observation that the OCP values at the analytical interface are well-negative of RHE across all pH values (**Fig. 3d**) and the observation of vigorous  $H_2$  evolution at the analytical interface highlights that this interface is out of equilibrium relative to the  $H_2/H^+$  electrochemical couple, and implies that the H species that set the OCP are  $H_{OPD}$ .

Two possible charge transfer reactions involving  $H_{OPD}$  can be envisioned: PCET to form and remove  $H_{OPD}$  (forward and reverse Volmer reaction) or PCET to interconvert  $H_{OPD}$  and  $H_2$  (forward and reverse Heyrovsky reaction).



Thus, rigorously speaking, the OCP at the analytical interface samples a mixed potential of these two reaction steps. Importantly, electrons and protons are on the same side of both equilibria, and, thus, irrespective of the relative contribution of each, the OCP will display a Nernstian scaling with pH. However,  $H_{OPD}$  is a product of the Volmer reaction step and is, instead, a reactant in the Heyrovsky reaction step. Increasing currents passed at the H-pumping interface and the correspondingly increased  $H_{OPD}$  population leads to a negative shift in the OCP, suggesting that the OCP value is dominated by the Volmer and reverse Volmer reactions. Furthermore, the minority contribution from the Heyrovsky step to the measured OCP is consistent with previous studies invoking H-H recombination as the primary pathway for  $H_2$  release.<sup>7,31</sup>

Taken together, the foregoing observations and analysis lead us to propose the following mechanistic model. Negative polarization at the H-pumping interface drives H diffusion across the Pd membrane to form a non-equilibrium, steady-state  $H_{OPD}$  population at the analytical interface. This non-equilibrium H activity shifts the OCP via changes in the activity of H,  $a_H$ , in the potential-determining  $H_{OPD}/H^+$  redox couple. Referencing to RHE accounts for proton activity, and, thus, the OCP at the analytical interface vs the RHE potential provides a direct measure of the change in chemical potential of the surface H on Pd relative to its reference chemical potential at the RHE potential. Thus, given that the HER is a reductive process, the chemical overpotential,  $\eta_{\text{chemical}}$ , can be calculated directly as the magnitude of the OCP deviation from the RHE potential:

$$\eta_{\text{chemical}} = -E_{\text{analytical OCP}} (\text{V vs RHE})$$

(See Supplementary Discussion for a detailed thermodynamic treatment of  $\eta_{\text{chemical}}$  and  $\eta_{\text{charge transfer}}$ , and their relationship to the free energy changes of the Volmer and Tafel reaction steps).

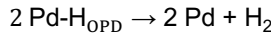
### Chemical Overpotential-Rate Scaling for H<sub>2</sub> Evolution is Insensitive to Reaction Conditions.

#### Chemical Overpotential-H<sub>2</sub> Evolution Rate Scaling is pH Independent.

The current passed at the H-pumping interface fractionates as H<sub>2</sub> evolution on both the H-pumping and analytical interface. Thus, the current passed at the H-pumping interface does not correspond to the rate of H<sub>2</sub> release at specifically the analytical interface where  $\eta_{\text{chemical}}$  is measured. To establish a scaling relationship for the chemical overpotential with the rate of the HER, we use in-line gas chromatography analysis (see SI for experimental details) to independently quantify the steady state rate of H<sub>2</sub> evolution at the analytical interface. To facilitate comparisons, rates of H<sub>2</sub> evolution were converted to a current density ( $j$ ) according to the following equation:

$$j = v_{\text{H}_2} \times nF$$

Here,  $v_{\text{H}_2}$  is the rate of H<sub>2</sub> evolution at the analytical interface in mol s<sup>-1</sup> cm<sup>-2</sup>,  $n$  is 2 due to the two electrons in each H<sub>2</sub> molecule, and  $F$  is the Faraday constant. Importantly, at open-circuit, there is no net Faradaic charge transfer across the analytical interface, and thus the H<sub>2</sub> release at this interface must proceed via the net recombination of H<sub>OPD</sub> species at the analytical interface:



We note that this reaction could proceed by the combination of reverse Volmer and forward Heyrovsky steps. However, our studies below suggest that this is a minor contributor to the mechanism of H<sub>2</sub> release. Furthermore, independent studies that analyze OCP decay transients also concluded that Tafel recombination is the primary pathway for H<sub>2</sub> release on Pd.<sup>7,31</sup>

We find that under all reaction conditions at the analytical interface, an increase in current passed at the H-pumping interface resulted in an increase in the steady state rates of H<sub>2</sub> release at the analytical interface (see **Fig. S2** for permeation rates). Importantly, under equivalent currents passed at the H-pumping interface, the rate of H<sub>2</sub> evolution is also largely insensitive to changes in pH. Increasing the electrolyte pH at the analytical interface results in only a small attenuation in H<sub>2</sub> release rates at the analytical interface, 24.4 mA cm<sup>-2</sup> in acid to 19.4 mA cm<sup>-2</sup> in base under a constant  $-100$  mA cm<sup>-2</sup> current passed at the H-pumping interface (see **Fig. S2**). By combining all the H<sub>2</sub> release rates at different pH values with their corresponding measured chemical overpotential, we are then able to examine the pH dependence of the  $\eta_{\text{chemical}}$ -rate scaling for H<sub>2</sub> release (**Fig. 4**). We find that, across 13 pH units, the  $\eta_{\text{chemical}}$ -rate scaling for H<sub>2</sub> release at the analytical interface is pH independent within error, with slopes ranging from 18-22 mV per decade and chemical overpotentials varying by  $< 4$  mV at equivalent H<sub>2</sub> release rates. Notably, increasing the membrane thickness from 25 to 100  $\mu\text{m}$  leads to a largely unchanged scaling of H<sub>2</sub> release rate with  $\eta_{\text{chemical}}$  (**Fig. S8**), suggesting that these trends reflect the interfacial H-H recombination kinetics rather than the rate of H-transport through the Pd membrane. Interestingly, this measured slope falls below the 30 mV dec<sup>-1</sup> slope predicted for H-H recombination controlled mechanisms with rate constants that are largely independent of surface H<sub>OPD</sub> coverage (see SI for detailed discussion).<sup>31</sup> The observed lower slope could result from a coverage dependent rate constant for H-H recombination and, indeed, a cooperative adsorption isotherm can lead to an increase in H-H recombination rate constant with coverage and a correspondingly attenuated slope (see **Fig. S6**).

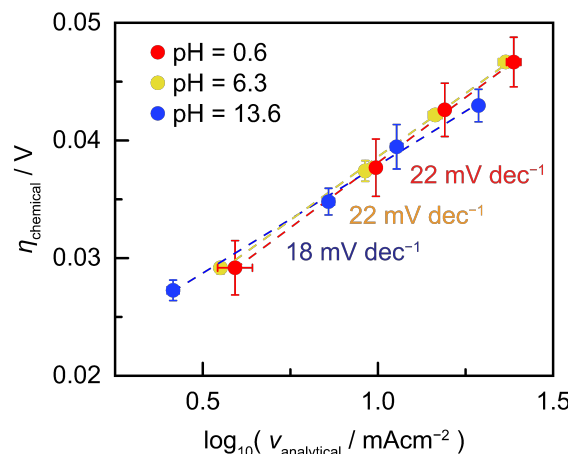


**Fig. 4 | pH-dependent rate scaling of H<sub>2</sub> release with chemical overpotential at the analytical interface.** The rate of H<sub>2</sub> release at the analytical interface ( $v_{\text{analytical}}$ ) versus the chemical overpotential at that interface ( $\eta_{\text{chemical}}$ ) under different pH conditions including 13.6 (blue), 6.3 (yellow) and 0.6 (red). Error bars indicate standard deviations obtained from three or more independent replicates (some error bars are smaller than the data point markers).

The invariance of the rate of the Tafel reaction with electrolyte pH under equivalent chemical overpotentials stands in stark contrast to the ~100 fold decrease in the rate of the overall HER from acid to base reported on Pd.<sup>11,15</sup> In our system, H<sub>2</sub> release occurs in the absence of net Faradaic charge transfer, thereby excluding any contribution from the charge transfer overpotential. This finding suggests that the pH dependence of HER efficiencies in conventional electrochemical systems arises almost exclusively from kinetic losses in PCET charge transfer steps (quantified explicitly below) rather than changes in the chemical reactivity of surface H. *Put simply, by supplying the key H<sub>OPD</sub> intermediates from the bulk of the Pd membrane, rather than via PCET from solution, the pH-dependent efficiency losses in H<sub>2</sub> evolution catalysis are almost entirely eliminated.*

*Chemical Overpotential-Rate Scaling is Independent of Surface Poisons or Promoter.*

Surface bound poisons and promoters are known to dramatically influence the overall kinetics of HER catalysis on noble metals. For example, adsorption of CO serves to strongly attenuate HER activity<sup>22–24</sup>, whereas islands of Ni(OH)<sub>2</sub> are known to promote HER rates in alkaline media.<sup>13,20,21</sup> However, it remains unclear whether these poisons and promoters augment HER rates via changes in the charge transfer kinetics, via changes to the kinetics of chemical reaction steps or some combination of both. Using the double cell methodology described above, we isolate the impact of CO and Ni(OH)<sub>2</sub> on the  $\eta_{\text{chemical}}$ -rate scaling for H<sub>2</sub> release.

To isolate the effect of CO, we introduced this poison to the analytical interface of the Pd electrochemical double cell with 1 M H<sub>2</sub>SO<sub>4</sub> in both compartments. Under reductive polarization of  $-100\text{ mA cm}^{-2}$  at the H-pumping interface, the introduction of 1 atm of CO to the analytical cell resulted, as expected, in an attenuation of the H<sub>2</sub> release rate at the analytical interface, decreasing from 24.4 to 9.2 mA cm<sup>-2</sup> (see **Fig. S4b**). This attenuation is consistent with CO binding to the analytical face to suppress H<sub>2</sub> release. Notably, the suppression in the H<sub>2</sub> release rate at the analytical interface with CO poisoning is also coupled to an attenuation of the chemical overpotential at that interface, shifting from 47 mV to 35 mV (see **Fig. S4a**). This trend of both H<sub>2</sub> release rates and  $\eta_{\text{chemical}}$  attenuating upon the addition of CO was observed across the entire range of currents sampled. Consequently, we find that the  $\eta_{\text{chemical}}$ -rate scaling for H<sub>2</sub> release is largely unaffected by the addition of CO (**Fig. 5a**). Thus, upon normalizing to an equivalent chemical overpotential of, for example, 30 mV, the rate of H<sub>2</sub> release between the CO poisoned and native Pd are largely unchanged at 4.74 and 4.29 mA cm<sup>-2</sup>, respectively. Additionally, the CO poisoned and native Pd display similar  $\eta_{\text{chemical}}$ -rate scaling factor for H<sub>2</sub> release of 22 and 19 mV dec<sup>-1</sup>, respectively (**Fig. 5a**). These data suggests that although CO binds to Pd surface sites and hinders the formation of H<sub>OPD</sub>, any interaction between CO and H<sub>OPD</sub> has no substantial impact on the rate constant for H<sub>OPD</sub> recombination to release H<sub>2</sub>. Rather, the poisoning effect of CO on the overall HER stems principally from an inhibition of the charge transfer kinetics for interfacial PCET (see below).

We also examined the effect of incorporating Ni(OH)<sub>2</sub> islands on the rate of H<sub>2</sub> release at the analytical interface. We deposited Ni(OH)<sub>2</sub> islands onto the analytical interface via Galvanostatic oxidative electrodeposition (see SI for details). In contrast to the behaviour observed upon addition of CO, the incorporation of Ni(OH)<sub>2</sub> does not substantially attenuate the H<sub>2</sub> release rate at the analytical interface relative to un-modified Pd interface (see **Fig. S5b**). Likewise, the addition of Ni(OH)<sub>2</sub> leads to no change in the OCP of the analytical interface within error (see **Fig. S5a**). Consistent with both of these observations, a plot of  $\eta_{\text{chemical}}$  vs the rate of H<sub>2</sub> release at the analytical interface overlays for the sample with and without Ni(OH)<sub>2</sub> (**Fig. 5b**). These data evince that the presence of Ni(OH)<sub>2</sub> negligibly affects the  $\eta_{\text{chemical}}$ -rate scaling for H<sub>2</sub> release. Rather, the promoting effect of Ni(OH)<sub>2</sub> stems principally from an enhancement in the charge transfer kinetic for interfacial PCET (see below). This observation is consistent with the trends previously observed for H<sub>UPD</sub> formation on Pt,<sup>13</sup> which invoke that Ni(OH)<sub>2</sub> islands are able to lower in the activation barrier for the Volmer reaction and have no impact to the energetics of the hydrogen intermediate or mechanism.

The foregoing studies highlight that both CO as a poison and Ni(OH)<sub>2</sub> as a promoter have minimal impact on the energetics associated with the chemical step of recombining H<sub>OPD</sub> species to form H<sub>2</sub>. Furthermore, similar to the above pH-dependence study, the absence of net charge transfer from the interface entirely eliminates the typical HER efficiency changes observed upon introduction of poisons or promoters.

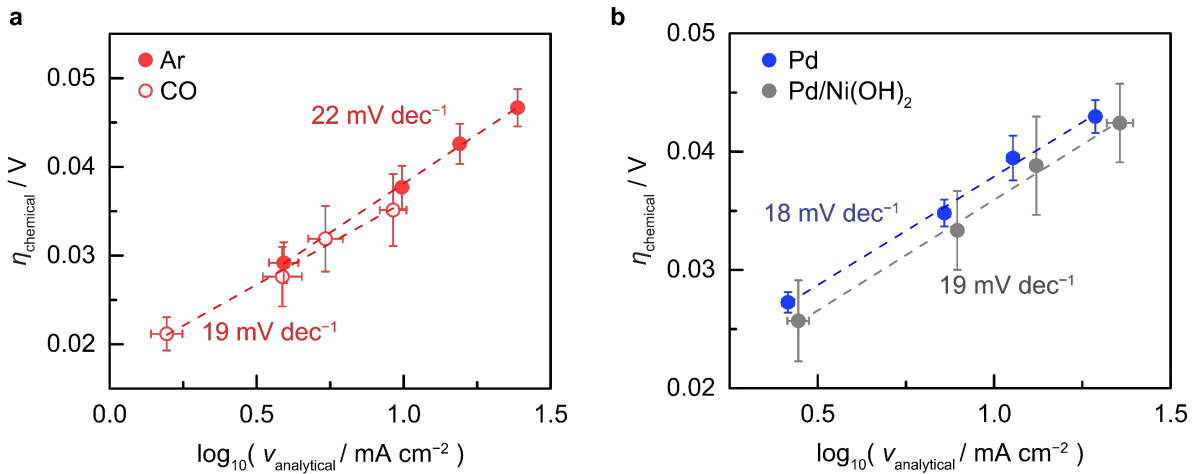


**Fig. 5 | The effect of CO and Ni(OH)<sub>2</sub> islands on the rate scaling of H<sub>2</sub> release with chemical overpotential at the analytical interface.** **a**, Rate of H<sub>2</sub> release at the analytical interface (v<sub>analytical</sub>) versus the chemical overpotential at that interface (η<sub>chemical</sub>) under an Ar atmosphere (solid red) and under a CO atmosphere (hollow red) (pH = 0.6). **b**, Rate of H<sub>2</sub> release at the analytical interface (v<sub>analytical</sub>) versus the chemical overpotential at that interface (η<sub>chemical</sub>) for both native Pd (blue) and Pd decorated with Ni(OH)<sub>2</sub> (grey) (pH = 13.6). Error bars indicate standard deviations obtained from two or more independent replicates (some error bars are smaller than the data point markers).

### Charge Transfer Overpotential for H<sub>2</sub> Catalysis is Highly Sensitive to Reaction Conditions.

#### Fixing the Chemical Overpotential Isolates Charge Transfer Kinetics.

The above data evinces that the η<sub>chemical</sub>-rate scaling for H<sub>2</sub> evolution is remarkably insensitive to changes in pH, the presence of surface poisons or the addition of surface promoters. Thus, these findings suggest that the strong reaction condition dependence of the overall HER reaction arise from changes in the charge transfer kinetics associated with the formation and removal of H<sub>OPD</sub>. To test this hypothesis, we super-imposed a small polarization at the analytical interface on top of a large background rate of H-pumping. Specifically, in all experiments, we set the current passed at the H-pumping interface to  $-100 \text{ mA cm}^{-2}$ , which generates an elevated chemical overpotential at the analytical interface and corresponding steady state rate of H<sub>2</sub> evolution in the analytical cell. During this background H<sub>2</sub> evolution process, we additionally polarized the analytical interface via electrical current flow from the external circuit in the analytical electrochemical cell. In the limit that the charge transfer rate at the analytical interface is small relative to the rate of H-transport from the opposite interface, the H<sub>OPD</sub> population, and thus the chemical overpotential at the analytical interface should be minimally perturbed. By holding the chemical overpotential roughly constant, the current potential relationship at the analytical interface should primarily sample the charge transfer kinetics. We apply this methodology to isolate and quantify the medium dependence of the charge transfer steps of hydrogen evolution catalysis.

#### Charge Transfer Overpotential Increases with Solution Alkalinity

We quantified the current-η<sub>charge transfer</sub> relationship across a variety of pH values while holding the pH of the H-pumping interface constant at 1 M H<sub>2</sub>SO<sub>4</sub>. With the H-pumping interface polarized Galvanostatically at  $-100 \text{ mA cm}^{-2}$ , we recorded a series of stepped Galvanostatic electrolyses in the analytical cell with current densities ranging from  $-3$  to  $3 \text{ mA cm}^{-2}$  to generate Butler-Volmer (BV) plots of the charge transfer kinetics. Under these conditions, the background rate of H<sub>2</sub> evolution at the analytical interface from H-permeation across the membrane reaches  $\sim 23 \text{ mA cm}^{-2}$ . Thus, the small additional current passed is expected to minimally perturb the H<sub>OPD</sub> population and corresponding chemical overpotential. We note that extending the range of currents passed at the analytical interface to  $\pm 30 \text{ mA cm}^{-2}$  did not appear to significantly impact the BV plots, and is likely a due to the far greater overpotential-rate scaling observed for η<sub>charge transfer</sub> compared to η<sub>chemical</sub>.

We first compared BV plots across acid, neutral, and basic electrolyte conditions. Under all pH conditions, the BV plots converge in the limit of zero current to around  $-45 \text{ mV}$  vs RHE, which is in close agreement to the chemical overpotential fixed by H-pumping to the analytical interface. Under acidic electrolyte conditions (Fig. 6, red), we observe charge transfer overpotentials of 5 and 7 mV for anodic and cathode current densities of  $3 \text{ mA cm}^{-2}$ ,

respectively. These charge transfer overpotentials increase with electrolyte pH, rising to 67 and 58 mV under near neutral conditions (**Fig. 6**, yellow) and increasing further to 294 and 226 mV under alkaline conditions (**Fig. 6**, blue). Fitting these data to the Butler-Volmer equation (see **Fig. S3**) returns exchange current densities of 14, 7.6, and 0.21 mA cm<sup>-2</sup> for solution pH values of 0.6, 6.3, and 13.6 respectively (see SI for details of the fitting procedure). This dramatic attenuation in charge transfer kinetics contrasts with the invariance of the  $\eta_{\text{chemical}}$ -rate scaling across the same range of pH (**Fig. 4**). Notably, the ~70 fold attenuation in charge transfer kinetics between acid and base is similar to the ~100 fold rate change in overall HER kinetics between acidic and alkaline conditions on Pd,<sup>11,15</sup> suggesting that the *pH-dependent kinetics of HER accrue almost entirely from changes in the rate of charge transfer rather than changes in the rate of surface chemical reactions*. The foregoing data on H<sub>OPD</sub> also follows the same trend as previous reports studying strongly bound H<sub>UPD</sub> species, on Pt, which have reported significant increases in the charge transfer resistance for the Volmer step with increasing electrolyte alkalinity.<sup>13</sup> Furthermore, the strong reaction condition dependence of the reverse Volmer reaction as shown in the anodic portion of the BV plot adds further insights into the H-H recombination pathway at the analytical interface. If H-H recombination at the analytical interface were to proceed via the combination of reverse Volmer and forward Heyrovsky steps, we would expect an analogous reaction condition dependent- $\eta_{\text{chemical}}$  scaling with H<sub>2</sub> release to that observed for the reverse Volmer reaction. This is at odds with the largely reaction condition independence observed (**Fig. 4**), bolstering the notion that H<sub>2</sub> release at the analytical interface proceeds primarily through a Tafel recombination mechanism involving no charge transfer steps.

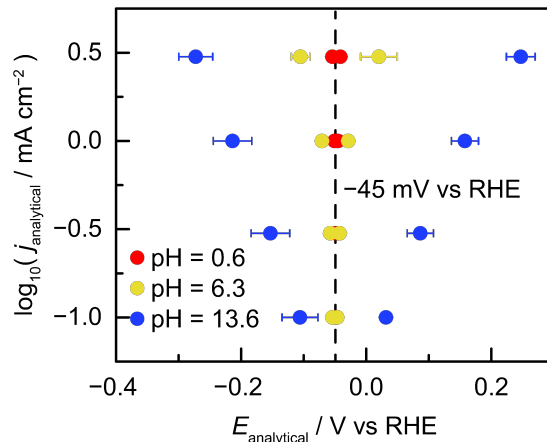


**Fig. 6 | Isolating the charge transfer overpotential component for passing current at the analytical interface.** Butler-Volmer behaviour for HER/HOR on the Pd analytical interface under a constant current density of  $-100 \text{ mA cm}^{-2}$  passed at the H-pumping interface. Note that both the x and y axis refer to the potential measured ( $E_{\text{analytical}}$ ) and the current density passed ( $j_{\text{analytical}}$ ) at the analytical interface respectively. Different pH conditions at the analytical interface including 13.6 (blue), 6.3 (yellow) and 0.6 (red). Error bars indicate standard deviations obtained from three or more independent replicates (some error bars are smaller than the data point markers).

#### Charge Transfer Overpotential is Highly Sensitive to the Surface Population of Promoters or Poisons.

Carbon monoxide is known to bind strongly to Pd surfaces and attenuate the rate of HER. We applied the above methodology to isolate how the  $\eta_{\text{charge transfer}}$ -rate scaling for the HER changes upon addition of CO. Upon addition of 1 atm of CO to 1 M H<sub>2</sub>SO<sub>4</sub> electrolyte, the charge transfer overpotential necessary to pass  $-3 \text{ mA cm}^{-2}$  substantially increases from 7 mV (**Fig. 7a**, solid red) to 260 mV (**Fig. 7a**, open red). This also corresponds to an ~100 fold suppression in the rate of charge transfer at the same overpotential (**Fig. 7a**). In contrast, for the same  $3 \text{ mA cm}^{-2}$  rate of H<sub>2</sub> evolution on the analytical interface at OCP, we measure a chemical overpotential of ~30 mV both in the presence and absence of CO. These findings suggest that the presence of a CO poison serve to predominantly attenuate  $\eta_{\text{charge transfer}}$  for forming H<sub>OPD</sub>, but minimally impacts  $\eta_{\text{chemical}}$ .

Analogously, the deposition of islands of Ni(OH)<sub>2</sub> is known to promote HER in alkaline media on noble metals. We applied the above methodology to isolate the effect of Ni(OH)<sub>2</sub> on the charge transfer kinetics of the HER. The incorporation of Ni(OH)<sub>2</sub> onto Pd lowered the charge transfer overpotential necessary to pass  $3 \text{ mA cm}^{-2}$  from 226 to 94 mV and 294 to 154 mV for H<sub>OPD</sub> generation and removal, respectively (**Fig. 7b**). Across the entire range of current

densities sampled, the reduction in the charge transfer overpotential corresponded to a 6- to 10-fold enhancement in rate at a common overpotential (**Fig. 7b**), which is in line with the 5- to 8-fold activity enhancement previously reported for  $\text{Ni(OH)}_2$  modified Pt surfaces.<sup>13,20</sup> Again, the strong effect that  $\text{Ni(OH)}_2$  has on the charge transfer kinetics stands in stark contrast with the largely invariant  $\eta_{\text{chemical}}$ -rate scaling for  $\text{H}_2$  release. Taken together, these data reveal that the HER promotion effects observed from the addition of  $\text{Ni(OH)}_2$  on Pd serve to improve the charge transfer kinetics for HER without affecting the  $\eta_{\text{chemical}}$ -rate scaling for  $\text{H}_2$  release.

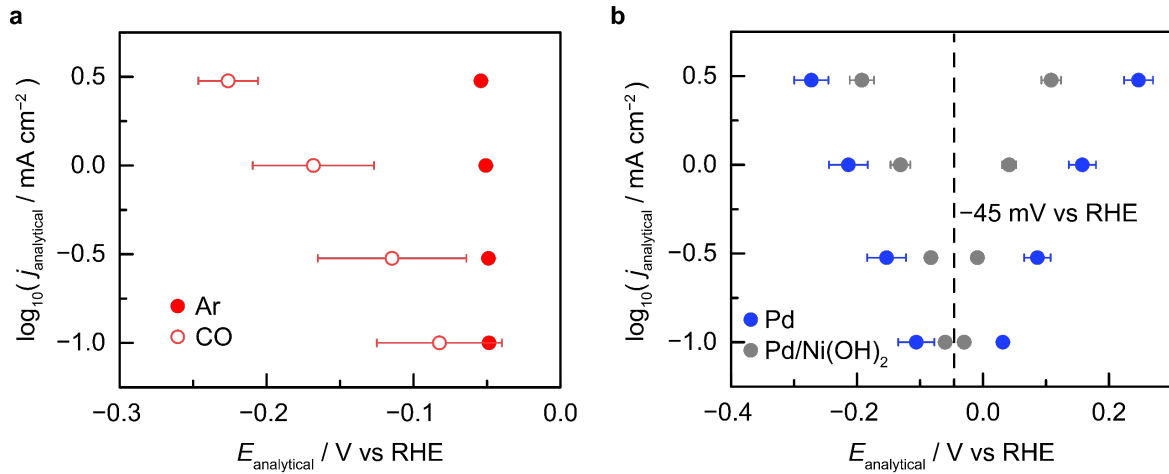


**Fig. 7 | The effect of CO as a poison and  $\text{Ni(OH)}_2$  islands as a promoter on the charge transfer overpotential component for passing current at the analytical interface. a**, Butler-Volmer behaviour for HER on the Pd analytical interface under a constant current density of  $-100 \text{ mA cm}^{-2}$  passed at the H-pumping for both Pd under an Ar (solid red) and CO atmosphere (hollow red), ( $\text{pH} = 0.6$ ). **b**, Butler-Volmer behavior for HER on the Pd analytical interface under a constant current density of  $-100 \text{ mA cm}^{-2}$  passed at the H-pumping interface for both native Pd (blue) and Pd decorated with  $\text{Ni(OH)}_2$  (grey) ( $\text{pH} = 13.6$ ). Error bars indicate standard deviations obtained from three or more independent replicates (some error bars are smaller than the data point markers).

#### Comparing the Chemical and Charge Transfer Overpotential Partitioning for Reaction Condition-Dependent HER Catalysis.

Aggregating the above data, we calculate the relative partitioning of the total overpotential into charge transfer and chemical contributions across all the conditions examined, at a common  $\text{H}_2$  generation rate of  $3 \text{ mA cm}^{-2}$  (**Fig. 8**). At steady state, the rate of chemical and charge transfer steps in a Volmer-Tafel mechanism are balanced with each other and to the overall rate of  $\text{H}_2$  generation such that the  $\text{H}_{\text{OPD}}$  coverage is unchanged. The data in **Fig. 4** and **5** provide the chemical overpotential, whereas the data in **Fig. 6** and **7** provide the charge transfer overpotential required for a given current density of  $\text{H}_2$  evolution. At  $\text{pH} 0.6$  we find that the chemical overpotential (30 mV) is substantially greater than the charge transfer overpotential (7 mV) (**Fig. 8**). This adds nuance to the general mechanistic consensus that the chemical step for H-H recombination limits the rate of HER catalysis in acidic aqueous media.<sup>8,13,45</sup> Indeed prior work has reported Tafel slopes as low as  $30 \text{ mV dec}^{-1}$  for the overall HER on Pd in acid.<sup>45</sup> Such low Tafel slopes have been interpreted as a Volmer-Tafel mechanism with a rate-limiting Tafel step, implying that all the overpotential for the HER in acid arises from chemical overpotential with no charge transfer overpotential contribution. Our data suggests a more nuanced explanation: both charge transfer (Volmer) and chemical reaction (Tafel) steps contribute to the overpotential of HER in acid, and the  $20 \text{ mV dec}^{-1}$  scaling of the latter (**Fig. 4**) combines with the charge transfer overpotential contribution to give rise to the  $30 \text{ mV dec}^{-1}$  Tafel slope for the overall reaction. Indeed for the H-pumping interface, where both charge transfer and chemical overpotentials are contribute, we too observe a Tafel slope of  $30 \text{ mV/decade}$  (**Fig. S9**).

The charge transfer overpotential contribution to the overall HER is far more amplified at elevated pH. At  $\text{pH} 6.3$  the chemical overpotential constitutes a minority fraction of the overall overpotential due to the substantial attenuation in charge transfer kinetics. This trend becomes even more pronounced at  $\text{pH} 13.6$ , where the 225 mV charge transfer overpotential dwarfs the measured 28 mV chemical overpotential (**Fig. 8**). The invariance of the chemical overpotential across the entire pH range combined with the large change in the charge transfer overpotential provides the clearest evidence to date that HER efficiency losses stem predominantly, if not exclusively, from changes in charge

transfer kinetics. Numerous previous studies have examined the impact of electrolyte cations and buffering species on HER kinetics,<sup>14,16–19,21</sup> and we posit that the methodology developed here can be readily extended to isolate the relative chemical and charge transfer overpotential contributions in each case. Furthermore, whilst these findings provide direct insight into the thermochemistry of  $\text{H}_{\text{OPD}}$  under HER conditions, it does not provide a measure of the surface coverage of  $\text{H}_{\text{OPD}}$ . Indeed, these studies could be coupled with operando infrared spectroscopy of the analytical interface to connect surface population and chemical potential of  $\text{H}_{\text{OPD}}$ , thereby providing a direct measure of the isotherm for kinetically competent H intermediates for the HER.

Even under acidic conditions, the addition of CO causes a remarkable attenuation in charge transfer kinetics, with an additional 250 mV of charge transfer overpotential necessary to pass 3 mA cm<sup>-2</sup> of HER current density. However, this change does not translate into any increase in the chemical overpotential for H-H recombination. Previous studies have examined co-adsorbate interactions between surface CO and surface H, but have led to conflicting conclusions suggesting both cooperative and inhibitory interactions.<sup>46–50</sup> While our finding would be consistent with a model in which adsorbed CO and  $\text{H}_{\text{OPD}}$  interact minimally, the data may also imply that CO preferentially binds to surface active site for the Volmer reaction and that distinct sites carry out H-H recombination. The methodology we develop here sets the stage for more detailed mechanistic and surface structural studies on the interplay of surface CO and H during HER catalysis. Expanding our analysis to an HER promoter, we find that under basic conditions, the high native charge transfer overpotential for the HER can be reduced on Pd by ~100 mV by depositing islands of  $\text{Ni(OH)}_2$  on the surface. However, similar to the addition of CO,  $\text{Ni(OH)}_2$  doesn't significantly alter the  $\eta_{\text{chemical-rate}}$  scaling for  $\text{H}_2$  release. This observation is consistent with previous studies on  $\text{H}_{\text{UPD}}$  formation, and how  $\text{Ni(OH)}_2$  islands on Pt are able to facilitate PCET for  $\text{H}_{\text{UPD}}$  formation, but have only nominal effects on the energetics and reactivity of surface H.<sup>13</sup> Taken together, these findings highlight the power of using the electrochemical double cell analysis to discriminate the chemical and charge transfer contributions to HER catalysis.

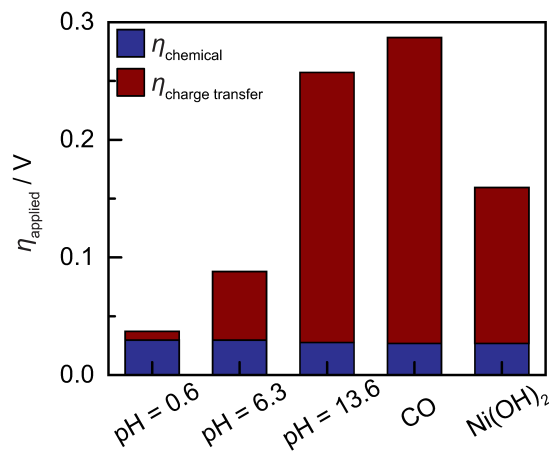


**Fig. 8 | Contribution of chemical and charge transfer overpotential for hydrogen catalysis under different reaction conditions.** The chemical (blue) and charge transfer (red) overpotential components for passing 3 mA cm<sup>-2</sup> of HER current density on Pd under different reaction conditions.

## CONCLUSION

This study reveals the importance of considering both the chemical and charge transfer overpotential components that make up electrocatalysis occurring at electrode interfaces. For the case of the HER, both the elevated, out of equilibrium chemical activity of  $\text{H}_{\text{OPD}}$  and the polarization necessary to drive charge transfer generate individual chemical and charge transfer overpotential components, respectively, to the aggregate overpotential. To isolate how changing reaction conditions independently tune both these components to affect overall HER efficiencies, we orthogonalize the delivery of  $\text{H}_{\text{OPD}}$  to a Pd surface using an electrochemical double cell system. In doing so, we are able to generate  $\text{H}_{\text{OPD}}$  without charge transfer to the interface of interest, and thus isolate the chemical overpotential for the HER. We are also able to further isolate the charge transfer overpotential component for the HER by maintaining an elevated chemical overpotential and further polarizing the Pd interface of interest.

Our principal findings can be summarized as follows. In all reaction conditions examined, the chemical overpotential-rate scaling for  $\text{H}_2$  release is largely unaffected by reaction conditions. Thus, by supplying the key  $\text{H}_{\text{OPD}}$

intermediate for HER without charge transfer at the interface, the reaction condition-dependence of H<sub>2</sub> generation is eliminated. Instead, the reaction condition-dependence of overall HER catalysis stems entirely from changes in the charge transfer overpotential, which are dramatically impacted. Bifurcating the overall overpotential into chemical and charge transfer components can guide catalyst design. For example, in acidic media, where PCET is rapid and the charge transfer overpotential is a minor component, the surface structure of the catalyst should be the primary target for optimization to reduce the chemical overpotential component. In contrast, under conditions where the charge transfer overpotential dominates, such as when poisoned by CO or when in alkaline media, design efforts should center on tuning the electrolyte and surface promoter composition to enhance PCET kinetics. By highlighting how different reaction conditions independently affect the chemical and charge transfer overpotential contributions to electrocatalysis occurring at electrode interfaces, these studies aim to reimagine future directed design of catalytic systems for improved efficiencies in electrochemical transformations.

#### Data Availability

The data that support the findings of this study are included in the published article (and its Supplementary Information) or available from the corresponding author on reasonable request.

### AUTHOR INFORMATION

#### Corresponding Author

\*yogi@mit.edu

#### Author Contributions

B.Y.T, R.P.B., and Y.S. conceived the research and developed experiments. B.Y.T conducted the majority of the experiments. R.P.B., K.M.L. and W.L.T. contributed to data collection. B.Y.T. and Y.S wrote the manuscript with input from all authors.

#### Competing Interests

The authors declare no competing financial interest.

#### Acknowledgement

We gratefully acknowledge Cyrille Costentin, Marc Koper, and James Mayer for fruitful discussions. The authors thank the entire Surendranath Lab for their support and scientific discussions, with particular acknowledgment towards H. Dinh, A. Chu, W. Howland, T. Marshall-Roth and H. Wang for their helpful discussions and mentorship. The authors would also like to thank C. Kaminsky and J. Ryu for their insights and mentorship. This research was supported by the National Science Foundation, under award number CHE-2102669.

### References

1. Seh, Z. W. *et al.* Combining theory and experiment in electrocatalysis: Insights into materials design. *Science* **355**, eaad4998 (2017).
2. Quaino, P., Juarez, F., Santos, E. & Schmickler, W. Volcano plots in hydrogen electrocatalysis – uses and abuses. *Beilstein J. Nanotechnol.* **5**, 846–854 (2014).
3. Tilak, B. V. & Conway, B. E. Analytical relations between reaction order and tafel slope derivatives for electrocatalytic reactions involving chemisorbed intermediates. *Electrochimica Acta* **37**, 51–63 (1992).
4. Conway, B. E. & Liu, T. C. Behaviour of surface intermediate states in anodic O<sub>2</sub> evolution electrocatalysis at Co<sub>3</sub>O<sub>4</sub> on Ni and Ti substrates. *Berichte Bunsenges. Für Phys. Chem.* **91**, 461–469 (1987).
5. Bockris, J. O. & Potter, E. C. The Mechanism of the Cathodic Hydrogen Evolution Reaction. *J. Electrochem. Soc.* **99**, 169 (1952).
6. Shinagawa, T., Garcia-Esparza, A. T. & Takanabe, K. Insight on Tafel slopes from a microkinetic analysis of aqueous electrocatalysis for energy conversion. *Sci. Rep.* **5**, 13801 (2015).
7. Enyo, M. & Maoka, T. The overpotential components on the palladium hydrogen electrode. *J. Electroanal. Chem. Interfacial Electrochem.* **108**, 277–292 (1980).
8. Enyo, M. & Maoka, T. The hydrogen electrode reaction mechanism on palladium and its relevance to hydrogen sorption. *Surf. Technol.* **4**, 277–290 (1976).
9. Green, J. a. S. & Lewis, F. A. Overvoltage component at palladized cathodes of palladium and palladium alloys prior to and during bubble evolution. *Trans. Faraday Soc.* **60**, 2234–2243 (1964).
10. Sheng, W. *et al.* Correlating hydrogen oxidation and evolution activity on platinum at different pH with measured hydrogen binding energy. *Nat. Commun.* **6**, 5848 (2015).
11. Zheng, J., Sheng, W., Zhuang, Z., Xu, B. & Yan, Y. Universal dependence of hydrogen oxidation and evolution reaction activity of platinum-group metals on pH and hydrogen binding energy. *Sci. Adv.* **2**, e1501602.

12. Chen, X., McCrum, I. T., Schwarz, K. A., Janik, M. J. & Koper, M. T. M. Co-adsorption of Cations as the Cause of the Apparent pH Dependence of Hydrogen Adsorption on a Stepped Platinum Single-Crystal Electrode. *Angew. Chem. Int. Ed.* **56**, 15025–15029 (2017).
13. Ledezma-Yanez, I. *et al.* Interfacial water reorganization as a pH-dependent descriptor of the hydrogen evolution rate on platinum electrodes. *Nat. Energy* **2**, 1–7 (2017).
14. Jung, O., Jackson, M. N., Bisbey, R. P., Kogan, N. E. & Surendranath, Y. Innocent buffers reveal the intrinsic pH- and coverage-dependent kinetics of the hydrogen evolution reaction on noble metals. *Joule* **6**, 476–493 (2022).
15. Durst, J. *et al.* New insights into the electrochemical hydrogen oxidation and evolution reaction mechanism. *Energy Environ. Sci.* **7**, 2255–2260 (2014).
16. Jackson, M. N., Jung, O., Lamotte, H. C. & Surendranath, Y. Donor-Dependent Promotion of Interfacial Proton-Coupled Electron Transfer in Aqueous Electrocatalysis. *ACS Catal.* **9**, 3737–3743 (2019).
17. Goyal, A. & Koper, M. T. M. The Interrelated Effect of Cations and Electrolyte pH on the Hydrogen Evolution Reaction on Gold Electrodes in Alkaline Media. *Angew. Chem. Int. Ed.* **60**, 13452–13462 (2021).
18. Monteiro, M. C. O., Goyal, A., Moerland, P. & Koper, M. T. M. Understanding Cation Trends for Hydrogen Evolution on Platinum and Gold Electrodes in Alkaline Media. *ACS Catal.* **11**, 14328–14335 (2021).
19. Huang, B. *et al.* Cation- and pH-Dependent Hydrogen Evolution and Oxidation Reaction Kinetics. *JACS Au* **1**, 1674–1687 (2021).
20. Subbaraman, R. *et al.* Enhancing Hydrogen Evolution Activity in Water Splitting by Tailoring Li<sup>+</sup>-Ni(OH)<sub>2</sub>-Pt Interfaces. *Science* **334**, 1256–1260 (2011).
21. McCrum, I. T. & Koper, M. T. M. The role of adsorbed hydroxide in hydrogen evolution reaction kinetics on modified platinum. *Nat. Energy* **5**, 891–899 (2020).
22. Leiva, E. P. M., Santos, E. & Iwasita, T. The effect of adsorbed carbon monoxide on hydrogen adsorption and hydrogen evolution on platinum. *J. Electroanal. Chem. Interfacial Electrochem.* **215**, 357–367 (1986).
23. Ji, S. G., Kim, H., Park, C., Kim, W. & Choi, C. H. Underestimation of Platinum Electrocatalysis Induced by Carbon Monoxide Evolved from Graphite Counter Electrodes. *ACS Catal.* **10**, 10773–10783 (2020).
24. Rodriguez, P., Feliu, J. M. & Koper, M. T. M. Unusual adsorption state of carbon monoxide on single-crystalline gold electrodes in alkaline media. *Electrochem. Commun.* **11**, 1105–1108 (2009).
25. Zeradjanin, A. R., Grote, J.-P., Polymeros, G. & Mayrhofer, K. J. J. A Critical Review on Hydrogen Evolution Electrocatalysis: Re-exploring the Volcano-relationship. *Electroanalysis* **28**, 2256–2269 (2016).
26. Kunimatsu, K., Senzaki, T., Samjeské, G., Tsushima, M. & Osawa, M. Hydrogen adsorption and hydrogen evolution reaction on a polycrystalline Pt electrode studied by surface-enhanced infrared absorption spectroscopy. *Electrochimica Acta* **52**, 5715–5724 (2007).
27. Zhu, S., Qin, X., Yao, Y. & Shao, M. pH-Dependent Hydrogen and Water Binding Energies on Platinum Surfaces as Directly Probed through Surface-Enhanced Infrared Absorption Spectroscopy. *J. Am. Chem. Soc.* **142**, 8748–8754 (2020).
28. Harrington, D. A. & Conway, B. E. Kinetic theory of the open-circuit potential decay method for evaluation of behaviour of adsorbed intermediates: Analysis for the case of the H<sub>2</sub> evolution reaction. *J. Electroanal. Chem. Interfacial Electrochem.* **221**, 1–21 (1987).
29. Conway, B. E. & Jerkiewicz, G. Relation of energies and coverages of underpotential and overpotential deposited H at Pt and other metals to the ‘volcano curve’ for cathodic H<sub>2</sub> evolution kinetics. *Electrochimica Acta* **45**, 4075–4083 (2000).
30. Conway, B. E. & Bai, L. State of adsorption and coverage by overpotential-deposited H in the H<sub>2</sub> evolution reaction at Au and Pt. *Electrochimica Acta* **31**, 1013–1024 (1986).
31. Maoka, T. & Enyo, M. Overpotential decay transients and the reaction mechanism on the Pd-H<sub>2</sub> electrode. *Surf. Technol.* **8**, 441–450 (1979).
32. Devanathan, M. a. V., Stachurski, Z. & Tompkins, F. C. The adsorption and diffusion of electrolytic hydrogen in palladium. *Proc. R. Soc. Lond. Ser. Math. Phys. Sci.* **270**, 90–102 (1962).
33. Ward, T. L. & Dao, T. Model of hydrogen permeation behavior in palladium membranes. *J. Membr. Sci.* **153**, 211–231 (1999).
34. Yun, S. & Ted Oyama, S. Correlations in palladium membranes for hydrogen separation: A review. *J. Membr. Sci.* **375**, 28–45 (2011).
35. Rahimpour, M. R., Samimi, F., Babapoor, A., Tohidian, T. & Mohebi, S. Palladium membranes applications in reaction systems for hydrogen separation and purification: A review. *Chem. Eng. Process. Process Intensif.* **121**, 24–49 (2017).
36. Delima, R. S., Sherbo, R. S., Dvorak, D. J., Kurimoto, A. & Berlinguette, C. P. Supported palladium membrane reactor architecture for electrocatalytic hydrogenation. *J. Mater. Chem. A* **7**, 26586–26595 (2019).
37. Jansonius, R. P. *et al.* Hydrogenation without H<sub>2</sub> Using a Palladium Membrane Flow Cell. *Cell Rep. Phys. Sci.* **1**, 100105 (2020).
38. Kurimoto, A., Sherbo, R. S., Cao, Y., Loo, N. W. X. & Berlinguette, C. P. Electrolytic deuteration of unsaturated bonds without using D<sub>2</sub>. *Nat. Catal.* **3**, 719–726 (2020).
39. Kurimoto, A. *et al.* Physical Separation of H<sub>2</sub> Activation from Hydrogenation Chemistry Reveals the Specific Role of Secondary Metal Catalysts. *Angew. Chem. Int. Ed.* **60**, 11937–11942 (2021).

40. S. Delima, R. *et al.* Selective hydrogenation of furfural using a membrane reactor. *Energy Environ. Sci.* **15**, 215–224 (2022).
41. Sherbo, R. S., Kurimoto, A., Brown, C. M. & Berlinguette, C. P. Efficient Electrocatalytic Hydrogenation with a Palladium Membrane Reactor. *J. Am. Chem. Soc.* **141**, 7815–7821 (2019).
42. Sherbo, R. S., Delima, R. S., Chiykowski, V. A., MacLeod, B. P. & Berlinguette, C. P. Complete electron economy by pairing electrolysis with hydrogenation. *Nat. Catal.* **1**, 501–507 (2018).
43. Yoshitake, H., Kikkawa, T. & Ota, K. Isotopic product distributions of CO<sub>2</sub> electrochemical reduction on a D flowing-out Pd surface in protonic solution and reactivities of “subsurface” hydrogen. *J. Electroanal. Chem.* **390**, 91–97 (1995).
44. Rock, P. A. Electrochemical double cells. *J. Chem. Educ.* **52**, 787 (1975).
45. Liu, S., Mu, X., Duan, H., Chen, C. & Zhang, H. Pd Nanoparticle Assemblies as Efficient Catalysts for the Hydrogen Evolution and Oxygen Reduction Reactions. *Eur. J. Inorg. Chem.* **2017**, 535–539 (2017).
46. Thrush, K. A. & White, J. M. Carbon monoxide and hydrogen coadsorption on polycrystalline platinum. *Appl. Surf. Sci.* **24**, 108–120 (1985).
47. Roman, T., Nakanishi, H. & Kasai, H. Coadsorbed H and CO interaction on platinum. *Phys. Chem. Chem. Phys.* **10**, 6052–6057 (2008).
48. Couple, J. & Bianchi, D. Experimental microkinetic approach of the CO/H<sub>2</sub> reaction on Pt/Al<sub>2</sub>O<sub>3</sub> using the Temkin formalism. 1. Competitive chemisorption between adsorbed CO and hydrogen species in the absence of reaction. *J. Catal.* **352**, 672–685 (2017).
49. Palazov, A., Kadinov, G., Bonev, Ch. & Shopov, D. Infrared spectroscopic study of the interaction between carbon monoxide and hydrogen on supported palladium. *J. Catal.* **74**, 44–54 (1982).
50. Yu, W.-Y., Mullen, G. M. & Mullins, C. B. Interactions of Hydrogen and Carbon Monoxide on Pd–Au Bimetallic Surfaces. *J. Phys. Chem. C* **118**, 2129–2137 (2014).

## Supporting Information

# Reaction Environment Impacts Charge Transfer But Not Chemical Reaction Steps in Hydrogen Evolution Catalysis

Bryan Y. Tang, Ryan P. Bisbey, Kunal M. Lodaya, Wei Lun Toh, Yogesh Surendranath\*

*Department of Chemistry, Massachusetts Institute of Technology,  
Cambridge, Massachusetts 02139*

yogi@mit.edu

<i>Index</i>	<i>Page</i>
<b>Experimental details</b>	S3–S8
<b>Supplementary Discussion</b>	S9–13
<b>Figure S1.</b> Illustrations and photographs of the electrochemical double cell configuration in a 2 compartment, 3 compartment and 4 compartment configuration	S14
<b>Figure S2.</b> pH dependent rate of H <sub>2</sub> release at the analytical interface ( $v_{An\ Tafel}$ ) against the total reductive current passed at the H-pumping interface ( $j_{H-P}$ ) under different pH	S15
<b>Figure S3.</b> Fitting the double polarization Butler-Volmer plots	S16
<b>Figure S4.</b> CO poisoning effects on the Pd electrochemical double cell measurements	S17
<b>Figure S5.</b> Effect of Ni(OH) <sub>2</sub> deposition on Pd electrochemical double cell measurements	S18
<b>Figure S6.</b> Modelling of a non-Langmrian isotherm and the effects of the Tafel desorption Tafel slope	S19
<b>Figure S7.</b> Open circuit potential decay transient of both the H-pumping and analytical interface post electrolysis	S20
<b>Figure S8.</b> Effect of Pd foil thickness on the scaling of chemical overpotential with H <sub>2</sub> release at the open circuit potential	S21
<b>S9.</b> Potential-current relationship observed at the H-pumping interface when the analytical interface is held at the open circuit potential.	S22
<b>Supplementary References</b>	S23

## Experimental Methods

**Materials.** Palladium foil (99.9%, 0.025 mm thickness) was purchased from Alfa Aesar and pre-treated according to the procedure below. Nickel chloride hexahydrate (99.95%) was obtained from Alpha Aesar and used as received. Palladium (II) sulfate dihydrate (98%) was obtained from Strem Chemicals and used as received. Hydrochloric acid (37 wt.%, 99.999% trace metal basis), sulfuric acid (95.5–96.5%, OmniTrace), lithium hydroxide (99.99%, semiconductor grade) and sodium hydroxide (99.99%, semiconductor grade), sodium perchlorate (99.95%) sodium phosphate dibasic dihydrate (> 99%), sodium phosphate monobasic monohydrate (> 99.5%) and Nafion 117 were obtained from Millipore Sigma and were used as received. Selemion (AMVN, AGC Inc.) was obtained from and soaked in 1 M NaOH for up to 24 h prior to use. Argon (UHP) and hydrogen gas (UHP) were obtained from Airgas and used as received. MilliQ water (Millipore Type 1, 18.2 MΩ cm) was used to make all electrolytes.

**General Electrochemical Methods.** Biologic VMP 16-channel potentiostats were used for all electrochemical experiments. Ag/AgCl reference electrodes were obtained from BASi Inc. (3 M NaCl) and eDAQ (leakless, ET069). Pt/C (0.5 mg cm<sup>-2</sup>) gas diffusion electrodes (GDE) were obtained from Fuel Cell Store. Alicat mass flow controllers were used to control gas flow rates to each electrochemical compartment. In all experiments, each solution was sparged with Ar at 10 sccm for at least 30 minutes before any polarization to remove dissolved oxygen from the electrolyte. Electrochemical studies were carried out using custom built gas-tight, glass H-cell parts. All experiments involved the use of two different three-electrode setups, with one comprising the H-pumping cell and the other comprising the analytical cell. The Pd foil membrane acted as the working electrode for both three-electrode setups. The geometric area of the Pd foil was controlled by the o-ring gasket of H-cell joint and was 1 cm<sup>2</sup>. All current densities are normalized to this geometric footprint rather than electrochemically active surface area. A Pt mesh or Pd foil was used as counter electrodes (both of which returned identical results).

Three electrochemical cell configurations were used (**Fig. S1**). The first configuration (**Fig. S1a**) contained two separated three electrode cells (the H-pumping and analytical cells) with a common Pd membrane working electrode. For each three electrode cell, the working (Pd) and counter (Pd or Pt) electrodes were not separated by a membrane separator. The second configuration (**Fig. S1b**) contained a Nafion membrane separating working and counter compartments of the H-pumping cell; working and counter electrodes remained unseparated in the analytical cell. The third configuration (**Fig. S1c**) contained membrane separators between working and counter compartments in both the H-pumping and analytical cells. Nafion was employed as the separator when the electrolyte was acidic and neutral, and Selemion was employed for alkaline electrolytes. It was found that the inclusion of a membrane separator had no appreciable effect on the electrochemical response of the system, and, as such, most of the data were collected using no membrane separators in either the H-pumping or analytical cells (configuration in **Fig. S1a**). All cell components were cleaned prior to use by immersion in

concentrated sulfuric acid for at least 1 h, followed by copious rinsing with Milli-Q water and drying under flowing Ar.

During all experiments, the electrochemical double cell was placed on a VWR 200 Rocking Platform Shaker set to rock at setting 2 to dislodge H<sub>2</sub> bubbles generated at the Pd interface during electrolysis.

**In-Line Gas Quantitation.** H<sub>2</sub> gas emanating from the analytical compartment was quantified by in-line gas chromatography using an SRI Instruments, Multi-Gas Analyzer, Model 8610C equipped with a thermal conductivity detector and a 2 m ShinCarbon (Restek) column. For experiments containing CO, in-line H<sub>2</sub> quantitation was conducted using an in-line gas chromatograph (SRI Instruments, Multi-Gas Analyzer, Model 8610C) equipped with a thermal conductivity detector and two MolSieve 13X and Hayesep D columns connect in series.

**Palladium Preparation.** Pd foil electrodes were cleaned and palladized prior to use in the electrochemical double cell. For the cleaning step, the Pd membrane double cell was assembled, with a 1 cm<sup>-2</sup> geometric surface area of Pd exposed to the electrolyte in the analytical and H-pumping cells. Both sides of the Pd foil were first simultaneously cleaned by CV cycling in 1 M H<sub>2</sub>SO<sub>4</sub> electrolyte under a continuous 10 sccm Ar sparge. CV cycling commenced at the open circuit potential (OCP) scanning negative at 50 mV s<sup>-1</sup> scan rate. The electrode was cycled between 0.1 and 1.1 V vs. Ag/AgCl (3 M NaCl) for 100 cycles. This cleaning procedure was conducted using a Pt mesh or Pd foil counter electrode. Both sides of the foil were then thoroughly washed with Milli-Q water (without disassembling the double cell).

Following cleaning by CV cycling, the Pd foil was retained in the same electrochemical double cell, and both sides of the Pd working electrode were palladized. A fresh 15.9 mM PdSO<sub>4</sub> solution in 1 M HCl was used for each palladization preparation. A Ag/AgCl (3 M NaCl) electrode and a Pt mesh or Pd foil were used as the reference and counter electrodes respectively on each compartment. The H-pumping and analytical cell compartments were each filled with 10 mL of the palladization solution, and each face of the Pd working electrode was simultaneously polarized potentiostatically to -0.2 V versus Ag/AgCl (3 M NaCl) without iR compensation until 7.38 C cm<sup>-2</sup> of charged. The palladization procedure was carried out under a continuous 10 sccm Ar sparge. The palladized Pd foil was then thoroughly washed with Milli-Q water (without disassembling the double cell) and dried in flowing Ar.

**Electrochemical deposition of Ni(OH)<sub>2</sub> onto Pd.** The analytical compartment was charged with 10 mL of 0.005 M Ni(Cl)<sub>2</sub>•6H<sub>2</sub>O electrolyte. The palladized Pd foil was then Galvanostatically polarized at +400 μA for 15 minutes in a two-electrode setup with a Pt mesh as the counter electrode. The foil was then thoroughly washed with Milli-Q water (without disassembling the double cell) and dried in flowing Ar.

**Determining the chemical overpotential-rate scaling for H<sub>2</sub> release.** Measurements of the OCP at the analytical interface at varying currents passed at the H-pumping interface were performed with the following setup: For the H-pumping cell, a Ag/AgCl (3 M NaCl) was used as the reference electrode and a Pt mesh or Pd foil was used as the counter electrode. In all experiments, the electrolyte used in the H-pumping cell was 1 M H<sub>2</sub>SO<sub>4</sub>. The H-pumping cell was also sparged with 10 sccm Ar, although replacing the gas with H<sub>2</sub> did not affect any of the measurements. For the analytical cell, a hanging strip Pt GDE was used as the reference electrode (which operates as a RHE when under an H<sub>2</sub> atmosphere) and either a Pt mesh or Pd foil was used as the counter electrode. The analytical cell was sparged with 10 sccm H<sub>2</sub>, although no difference in potential between the additional reference and the Pd working electrode was observed when H<sub>2</sub> was replaced with Ar (however, the Pt GDE would no longer be capable of acting as a reference electrode). Electrolytes used in the analytical cell included 1 M H<sub>2</sub>SO<sub>4</sub> (pH = 0.6), 1 M sodium hydroxide (pH = 13.6), 1 M lithium hydroxide (pH = 13.6), 0.5 M sodium formate + 0.5 M sodium borate + 1 M sodium perchlorate buffer (pH = 7.3), 0.5 M sodium acetate + 0.5 M sodium borate + 1 M sodium perchlorate buffer (pH = 7.3) and 1 M sodium phosphate + 1 M sodium perchlorate buffer (pH = 6.3) (**Fig. 3**). All experiments involving Ni(OH)<sub>2</sub> were conducted in 1 M sodium hydroxide (pH = 13.6) (**Fig. S5a**).

For measurement of the OCP of the analytical interface, the H-pumping interface was galvanostatically polarized at current densities ranging from  $-1$  to  $-100$  mA cm $^{-2}$ . During each galvanostatic electrolysis, the OCP was recorded in the analytical cell. Galvanostatic polarization on the H-pumping cell was held until the OCP at the analytical interface reached a stable value, which took anywhere from 1 to 20 minutes. These steady-state open circuit values at the analytical interface provided the X-axis data points in **Fig. 3** and **S5a** and **S6a**.

For measurements of the H<sub>2</sub> permeation rate at the analytical interface under Galvanostatic polarization at the H-pumping interface, the following set up was employed: For the H-pumping cell, a Ag/AgCl (3 M NaCl) was used as the reference electrode and a Pt mesh or Pd foil was used as the counter electrode. A three-compartment cell was used such that the working and counter electrodes of the H-pumping cell were separated by a Nafion membrane. The electrolyte used was 1 M H<sub>2</sub>SO<sub>4</sub> in all experiments. For the analytical cell, a Ag/AgCl (3 M NaCl in acid and neutral electrolytes, leakless in alkaline electrolytes) was used as the reference electrode and either a Pt mesh or Pd foil was used as the counter electrode. Both cells were sparged independently with Ar at 10 sccm. The current density at the H-pumping interface ranged from  $-10$  to  $-100$  mA cm $^{-2}$ , and the analytical interface was held at the OCP for the duration of the experiment. The outflow of the analytical compartment was analyzed via GC to measure the amount of H<sub>2</sub> that permeated across the Pd membrane. In each experiment, galvanostatic electrolysis at the H-pumping interface was maintained for 30 minutes, which afforded enough time to reach a steady state H<sub>2</sub> evolution rate at analytical interface as judged by a stable GC response. The recorded OCP values at the analytical interface was converted to the reversible hydrogen electrode (RHE) scale using the following equation, ( $E_{\text{RHE}} = E_{\text{Ag/AgCl}} + 0.210 \text{ V} + 0.059V \times \text{pH}$ ), and were unchanged from the

potentials measured under a H<sub>2</sub> atmosphere using the RHE reference electrode in the experiments mentioned above.

H<sub>2</sub> evolution in analytical cell compartment was measured using an in-line gas chromatograph and detected using the equipped thermal conductivity detector. A 2 m ShinCarbon (Restek) column with an isothermal temperature program (165 °C) and Ar carrier gas (UHP, Airgas, 20 psi) were used to separate H<sub>2</sub> from possible contaminant gasses (O<sub>2</sub> or N<sub>2</sub>), which were not observed in the effluent from either cell. GC traces were collected every 3 min from a 0.5 mL sample loop injection. The concentration of H<sub>2</sub> was determined via integrated peak area via a calibration curve. The partial current density for H<sub>2</sub> was calculated using the following equation:

$$j_i = c_i * n_i * F * V_{\text{gas}} * \frac{P}{RT} * \frac{1}{A}$$

where c<sub>i</sub> is the GC detected product in ppm, n<sub>i</sub> is the electron stoichiometry for the H<sub>2</sub> product, 2, F is Faraday's constant (96485 C mol<sup>-1</sup>), V<sub>gas</sub> is the substrate gas flow rate (10 sccm in all cases), P is the pressure in the cell (1 atm), A is the sample surface area, R is the gas constant and T is temperatures.

To establish a chemical overpotential-rate scaling for H<sub>2</sub> release, the deviation of the OCP from RHE at the analytical interface (measured from OCP experiments under both a H<sub>2</sub> and Ar atmosphere) was plotted against the log rate of H<sub>2</sub> release measured at that same interface. Chemical overpotential-rate scaling for H<sub>2</sub> release relationships were obtained for electrolytes in the analytical cell including 1 M H<sub>2</sub>SO<sub>4</sub> acid (pH = 0.6), 1 M sodium hydroxide (pH = 13.6), and 1 M sodium phosphate + 1 M sodium perchlorate buffer (pH = 6.3). The forgoing procedure generated the data in **Fig. 4**. All experiments involving Ni(OH)<sub>2</sub> were conducted in 1 M NaOH and generated the data in **Fig. 5b**.

**Determining the chemical overpotential-rate scaling for H<sub>2</sub> release in the presence of CO.** For studies that examined the effect of CO poisoning on the Pd membrane double cell, slight modifications to the above method were applied: The electrolyte used in both the H-pumping and analytical cell was 1 M H<sub>2</sub>SO<sub>4</sub>. For the H-pumping cell, a Ag/AgCl (3 M NaCl) was used as the reference electrode and a Pt mesh or Pd foil was used as the counter electrode. The H-pumping cell was sparged with 10 sccm Ar for the duration of the experiment. For the analytical cell, a Ag/AgCl (3 M NaCl) was used as the reference electrode and either a Pt mesh or Pd foil was used as the counter electrode. The analytical cell was initially sparged with 10 sccm Ar, and switched to 20 sccm CO during the course of the experiment. To measure the chemical overpotential, galvanostatic polarization with current densities ranging from -1 to -100 mA cm<sup>-2</sup> was performed at the H-pumping cell, and the OCP was measured on the analytical cell (**Fig. S4a**). Galvanostatic polarizations on the H-pumping cell was held until the open circuit response stabilized, which took anywhere from 1 to 20 minutes. The recorded OCP values at the analytical interface was converted to the reversible hydrogen electrode (RHE) scale using the following equation, (E<sub>RHE</sub> = E<sub>Ag/AgCl</sub> + 0.210 V + 0.059V × pH).

The same cell setup was used to measure H<sub>2</sub> permeation rates at the analytical interface under CO poisoning conditions. H<sub>2</sub> was measured using an in-line gas chromatograph and detected using the equipped thermal conductivity detector. Both cells were initially sparged independently with Ar at 10 sccm. Then, the sparge gas in the analytical cell was switched to CO at 20 sccm. The current density at the H-pumping interface ranged from  $-10$  to  $-100$  mA cm<sup>-2</sup>, and the analytical interface was held at OCP for the duration of the experiment. The outflow of the analytical compartment was analyzed via gas chromatography to measure the amount of H<sub>2</sub> permeation across the Pd membrane. All gaseous products were identified and quantified following a GC analysis methodology described in the literature.<sup>1</sup> The partial current density for H<sub>2</sub> was calculated using the same above equation. Each H-pumping current was maintained for 40 minutes, which yielded a stable GC response for H<sub>2</sub> detection.

To establish a chemical overpotential-rate scaling for H<sub>2</sub> release with CO poisoning, the deviation of the OCP from RHE at the analytical interface was plotted against the log rate of H<sub>2</sub> release measured at that same interface to produce the plot in **Fig. 5a**.

#### **Isolating the charge transfer overpotential component for passing current at the analytical interface (with and without CO).**

For experiments isolating the charge transfer overpotential component for H<sub>2</sub> catalysis (**Fig. 6** and **Fig. 7**), simultaneous polarization of both the H-pumping and analytical interfaces of the Pd membrane was performed. In all experiments, the current density at the H-pumping interface was maintained at  $-100$  mA cm<sup>-2</sup>. Simultaneously, current was passed at the analytical interface. For experiments that did not involve CO (**Fig. 6** and **Fig. 7b**), the analytical compartment was sparged with H<sub>2</sub> at 10 sccm, and Pt GDE was used as the reference electrode. Current densities at the analytical interface ranged from  $-30$  to  $30$  mA cm<sup>-2</sup>, with galvanostatic polarization held until the potential at the analytical interface reached steady state (between 5–10 minutes). For unmodified Pd electrodes, the electrolytes used in the analytical cell included 1 M H<sub>2</sub>SO<sub>4</sub> acid (pH = 0.6), 1 M sodium hydroxide (pH = 13.6) and 1 M sodium phosphate + 1 M sodium perchlorate buffer (pH = 6.3) and produced the data in **Fig. 6**. All experiments involving Ni(OH)<sub>2</sub> modified Pd were conducted in 1 M sodium hydroxide (pH = 13.6) and produced the data in **Fig. 7b**. For experiments that involved CO, the analytical compartment was sparged with CO at 20 sccm and a Ag/AgCl (3 M NaCl) was used as a reference electrode. Current densities at the analytical interface ranged from  $-3$  to  $0$  mA cm<sup>-2</sup>. Oxidative currents could not be sampled under CO as measured potentials were unstable and did not reach steady state. This procedure generated the data in **Fig. 7a**.

Fitting of double polarization Butler-Volmer plots was performed in MATLAB (version 2021b) via a non-linear least squares method. The experimental current density ( $j$ ) and potential ( $E$ ) data were fit to the logarithm of the absolute value of the Butler-Volmer equation:

$$\log_{10}|j| = \log_{10} \left| j_0 e^{\alpha \frac{F(E-E_0)}{RT}} - j_0 e^{-(1-\alpha) \frac{F(E-E_0)}{RT}} \right|$$

where  $F$  is Faraday's constant,  $R$  is the ideal gas constant, and  $T$  is the temperature (300 K). The equilibrium potential ( $E_0$ ) exchange current density ( $j_0$ ), and the symmetry factor ( $\alpha$ ) were parameters determined from the fitting procedure. When the current density is large or more polarized, it is convoluted by a non-negligible shift in chemical overpotential at steady state. To minimize the effect of this convolution on the fit, the data points were weighted by the reciprocal of the absolute value of  $j$ . The average of the least polarized anodic and cathodic potentials was used as the starting value the equilibrium potential. A symmetry factor of 0.5 and current density of 1.0 nA cm<sup>-2</sup> were used for the other starting values. Data fitting was used to produce the plot in **Fig. S4**.

## **Supplementary Discussion**

*Definition of the Chemical Overpotential:*

We first define the chemical potential of H under non-equilibrium steady state catalysis in terms of the activity of H:

$$\mu_H = RT \ln a_H \quad \text{Eq. S1}$$

We define the standard state chemical potential,  $\mu_{H,0}$ , as the chemical potential of surface H in equilibrium with 1 atm of H<sub>2</sub>:

$$\mu_{H,0} = RT \ln a_{H,0} \quad \text{Eq. S2}$$

Combining Eq. S1 and S2:

$$\mu_H - \mu_{H,0} = RT \ln \frac{a_H}{a_{H,0}} \quad \text{Eq. S3}$$

This difference in chemical potential can be converted to voltage units by dividing by Faraday's constant,  $F$ , to arrive at the definition of chemical overpotential,  $\eta_{\text{chemical}}$  as given in Eq. 1 in the main text:

$$\eta_{\text{chemical}} = \frac{\mu_H - \mu_{H,0}}{F} = \frac{RT}{F} \ln \frac{a_H}{a_{H,0}} \quad \text{Eq. S4}$$

*Relating the Open Circuit Potential at the Analytical Interface to the Chemical Overpotential for HER.*

In a Volmer-Tafel mechanism, there are two steps, each of which have their own distinct electrochemical free energies  $\Delta\bar{G}$ . For the Volmer reaction,  $\Delta\bar{G}_V$  can be expressed with the following relationship:

$$\Delta\bar{G}_V = \Delta G_V + FE = \Delta G_V^0 + FE - RT \ln \left( \frac{a_{H^+}}{a_H} \right) \quad \text{Eq. S5}$$

At standard state activity for H<sup>+</sup> and surface H, the last term cancels, giving:

$$\Delta\bar{G}_V = \Delta G_V^0 + FE \quad \text{Eq. S6}$$

At equilibrium,  $\Delta\bar{G}_V = 0$ , and  $E = E_{H^+/\text{H}_{\text{OPD}}}^0$ , thus,

$$\Delta G_V^0 = -FE_{H^+/\text{H}_{\text{OPD}}}^0 \quad \text{Eq. S7}$$

Similarly, for the Tafel reaction,  $\Delta\bar{G}_T$  can be expressed with the following relationship:

$$\Delta\bar{G}_T = \Delta G_T = \Delta G_T^0 - RT\ln\left(\frac{a_H}{(a_{H_2}^{0.5})_{eq}}\right) \quad \text{Eq. S8}$$

At equilibrium (i.e.  $\Delta\bar{G}_T = 0$ ), the activities of H<sub>2</sub> and surface H are equilibrated such that

$$0 = \Delta G_T^0 - RT\ln\left(\frac{a_{H,eq}}{(a_{H_2}^{0.5})_{eq}}\right) \quad \text{Eq. S9}$$

Rearranging **Eq. S9** provides an expression for  $\Delta G_T^0$ :

$$\Delta G_T^0 = RT\ln\left(\frac{a_{H,eq}}{(a_{H_2}^{0.5})_{eq}}\right) \quad \text{Eq. S10}$$

Substituting **Eq. S10** into **Eq. S8** yields the following relationship:

$$\begin{aligned} \Delta\bar{G}_T &= RT\ln\left(\frac{a_{H,eq}}{(a_{H_2}^{0.5})_{eq}}\right) - RT\ln\left(\frac{a_H}{a_{H_2}^{0.5}}\right) \\ -\Delta\bar{G}_T &= RT\ln\left(\frac{a_H}{a_{H,eq}} \times \frac{(a_{H_2}^{0.5})_{eq}}{a_{H_2}^{0.5}}\right) \end{aligned} \quad \text{Eq. S11}$$

Assuming that  $a_{H_2}^{0.5} = (a_{H_2}^{0.5})_{eq}$  (i.e. in the limit that the H<sub>2</sub> activity is unchanged in its out of equilibrium state), **Eq. S11** can be simplified to the following equation:

$$-\Delta\bar{G}_T = RT\ln\left(\frac{a_H}{a_{H,eq}}\right) \quad \text{Eq. S12}$$

Notably,  $a_{H,eq} = a_{H,0}$  when referencing to the equilibrium activity of surface H under 1 atm H<sub>2</sub> (under standard state conditions). Thus, the change in free energy for the Tafel step relative to the standard state conditions (1 atm H<sub>2</sub>), in the limit of unchanged H<sub>2</sub> activity can be expressed as:

$$-\Delta\bar{G}_T = RT\ln\left(\frac{a_H}{a_{H,0}}\right) \quad \text{Eq. S13}$$

**Eq. S13** with **Eq. S4** are related by the following expression:

$$\frac{-\Delta\bar{G}_T}{F} = \frac{RT}{F} \ln \frac{a_H}{a_{H,0}} = \eta_{chemical} \quad \text{Eq. S14}$$

The standard state potential for the overall HER can be obtained from the sum of the Volmer and Tafel free energy changes at standard state such that:

$$\Delta G_V^0 + \Delta G_T^0 = -FE_{\text{H}^+/\text{H}_2}^0 \quad \text{Eq. S15}$$

The measured OCP at the analytical interface is assumed to be set by the quasi-equilibrated Volmer reaction but at a non-equilibrium H activity relative to H<sub>2</sub>. Thus, the OCP reports on the deviation of the Volmer reaction from its standard state:

$$E_{OCP} = E_V = E_{\text{H}^+/\text{H}_{\text{OPD}}}^0 + \frac{RT}{F} \ln \left( \frac{a_{\text{H}^+}}{a_{\text{H}}} \right) \quad \text{Eq. S16}$$

Substituting in  $\Delta G_V^0 = -FE_{\text{H}^+/\text{H}_{\text{OPD}}}^0$ :

$$E_{OCP} = -\frac{\Delta G_V^0}{F} + \frac{RT}{F} \ln \left( \frac{a_{\text{H}^+}}{a_{\text{H}}} \right) \quad \text{Eq. S17}$$

Substituting in  $\frac{\Delta G_V^0}{F} = -\frac{\Delta G_T^0}{F} - E_{\text{H}^+/\text{H}_2}^0$  (from **Eq. S15**):

$$E_{OCP} = -\left( -\frac{\Delta G_T^0}{F} - E_{\text{H}^+/\text{H}_2}^0 \right) + \frac{RT}{F} \ln \left( \frac{a_{\text{H}^+}}{a_{\text{H}}} \right) \quad \text{Eq. S18}$$

This can be rearranged as:

$$E_{OCP} = -\left( -\frac{\Delta G_T^0}{F} + \frac{RT}{F} \ln(a_{\text{H}}) \right) + E_{\text{H}^+/\text{H}_2}^0 + \frac{RT}{F} \ln(a_{\text{H}^+}) \quad \text{Eq. S19}$$

Isolating  $\left( -\frac{\Delta G_T^0}{F} + \frac{RT}{F} \ln(a_{\text{H}}) \right)$  gives the following expression:

$$-\frac{\Delta G_T^0}{F} + \frac{RT}{F} \ln(a_{\text{H}}) = -\left( E_{OCP} - \left( E_{\text{H}^+/\text{H}_2}^0 + \frac{RT}{F} \ln(a_{\text{H}^+}) \right) \right) \quad \text{Eq. S20}$$

Subtracting  $\frac{RT}{F} \ln \left( (a_{\text{H}_2}^{0.5})_0 \right)$  on both sides yields:

$$-\frac{\Delta G_T^0}{F} + \frac{RT}{F} \ln \left( \frac{a_{\text{H}}}{(a_{\text{H}_2}^{0.5})_0} \right) = -\left( E_{OCP} - \left( E_{\text{H}^+/\text{H}_2}^0 + \frac{RT}{F} \ln \left( \frac{a_{\text{H}^+}}{(a_{\text{H}_2}^{0.5})_0} \right) \right) \right) \quad \text{Eq. S21}$$

In the limit that the activity of H<sub>2</sub> at the electrode surface is equal to the equilibrium value considered at RHE potential (i.e.  $a_{\text{H}_2}^{0.5} = (a_{\text{H}_2}^{0.5})_{eq} = (a_{\text{H}_2}^{0.5})_0$ ) **Eq. S8** can be rearranged and expressed in this system as:

$$\frac{\Delta \bar{G}_T}{F} = \frac{\Delta G_T^0}{F} - \frac{RT}{F} \ln \left( \frac{a_{\text{H}}}{(a_{\text{H}_2}^{0.5})_0} \right) \quad \text{Eq. S22}$$

Substituting **Eq. S22** into **Eq. S21** yields:

$$-\frac{\Delta\bar{G}_T}{F} = -\left( E_{OCP} - \left( E_{H^+/H_2}^0 + \frac{RT}{F} \ln \left( \frac{a_{H^+}}{(a_{H_2}^{0.5})_0} \right) \right) \right) \quad \text{Eq. S23}$$

Note that  $\left( E_{H^+/H_2}^0 + \frac{RT}{F} \ln \left( \frac{a_{H^+}}{(a_{H_2}^{0.5})_0} \right) \right)$  is the RHE potential, and thus,  $E_{OCP} - \left( E_{H^+/H_2}^0 + \frac{RT}{F} \ln \left( \frac{a_{H^+}}{(a_{H_2}^{0.5})_0} \right) \right)$  refers to the potential  $E_{OCP}$  against the RHE potential. Therefore:

$$-\frac{\Delta\bar{G}_T}{F} = -E_{OCP} \quad (V \text{ vs. RHE }) \quad \text{Eq. S24}$$

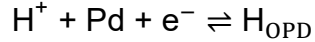
Finally, substituting  $-\frac{\Delta\bar{G}_T}{F} = \eta_{chemical}$  (Eq. S12) yields the following relationship:

$$\eta_{chemical} = -E_{OCP} \quad (V \text{ vs. RHE }) \quad \text{Eq. S25}$$

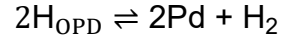
### Derivation of the Calculated 30 mV dec<sup>-1</sup> Tafel slope for a Tafel rate limiting mechanism

Consider the Volmer-Tafel Mechanism

Volmer step:



Tafel step (rate limiting step):



In a Tafel limited HER mechanism, we assume that the Volmer step is in equilibrium such that its potential can be described by the Nernst Equation:

$$\begin{aligned} E_V &= E_{\text{H}^+/\text{H}_{\text{OPD}}}^0 - \frac{RT}{F} \ln \left( \frac{a_{\text{H}}}{a_{\text{H}}^+} \right) \\ E_V &= E_{\text{H}^+/\text{H}_{\text{OPD}}}^0 - \frac{RT}{F} \ln(a_{\text{H}}) + \frac{RT}{F} \ln(a_{\text{H}}^+) \end{aligned} \quad \text{Eq. 26}$$

The rate of the HER, can also be described as the forward rate of the Tafel reaction:

$$i \times F = 2v_{\text{Tafel}} = k_{\text{Tafel}} a_{\text{H}}^2 \quad \text{Eq. 27}$$

Where  $i$  is the current passed and  $k_{\text{Tafel}}$  is the forward potential independent rate constant for the Tafel reaction. We assume there is no reverse Tafel process as Tafel is rate limiting.

**Eq. 27** can be rearranged to isolate  $a_{\text{H}}$ :

$$a_{\text{H}} = \left( i \times \frac{F}{k_{\text{Tafel}}} \right)^{0.5} \quad \text{Eq. 28}$$

Substituting **Eq. 28** into **Eq. 26** yields

$$E_V = E_{\text{H}^+/\text{H}_{\text{OPD}}}^0 - \frac{RT}{F} \ln \left( \left( i \times \frac{F}{k_{\text{Tafel}}} \right)^{0.5} \right) + \frac{RT}{F} \ln(a_{\text{H}}^+) \quad \text{Eq. 29}$$

The natural logarithm  $\frac{RT}{F} \ln(i^{0.5})$  can be approximated as  $\frac{0.059}{2} \log(i)$ , and thus **Eq. 29** can be rewritten in the following form:

$$E_V = E_{\text{H}^+/\text{H}_{\text{OPD}}}^0 - \frac{RT}{F} \ln \left( \left( \frac{F}{k_{\text{Tafel}}} \right)^{0.5} \right) + \frac{RT}{F} \ln(a_{\text{H}}^+) - \frac{0.059}{2} \log(i) \quad \text{Eq. 30}$$

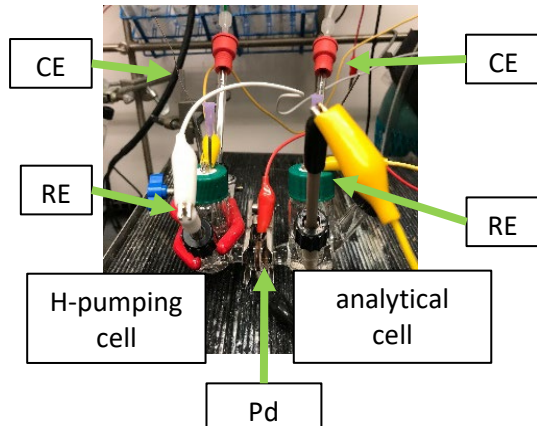
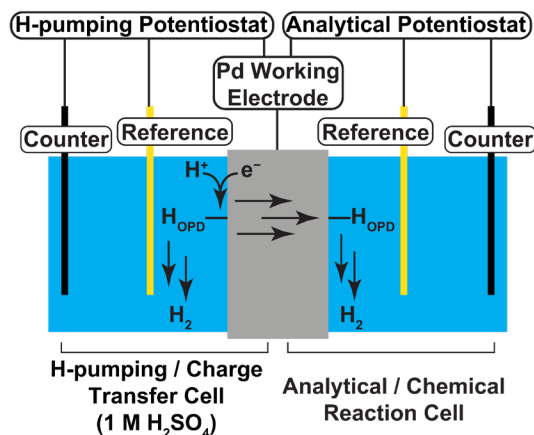
Taking the derivative of  $E_V$  with respects to  $\log(i)$  yields:

$$\frac{dE_V}{d \log(i)} = -\frac{0.059}{2} \text{ mV dec}^{-1} \quad \text{Eq. 31}$$

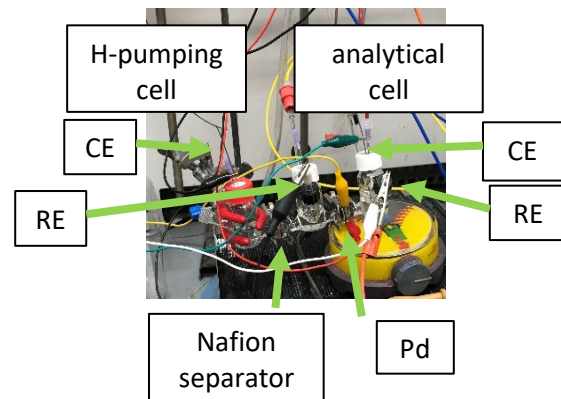
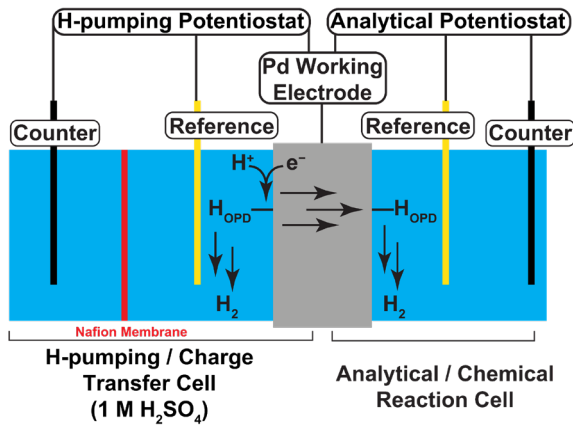
Thus, the Tafel slope,  $\left| \frac{dE}{d \log(i)} \right|$ , for a Tafel rate limiting mechanism of the HER is  $29.5 \approx 30 \text{ mV dec}^{-1}$

## Supplementary Figures

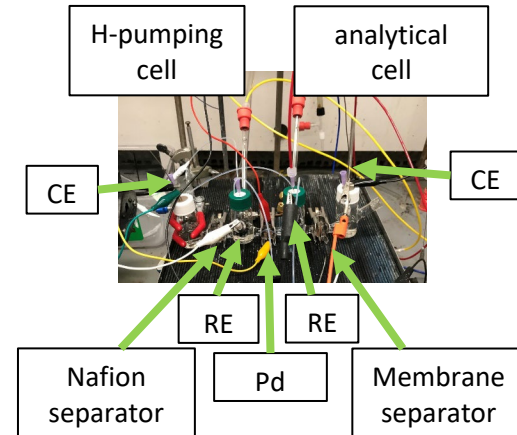
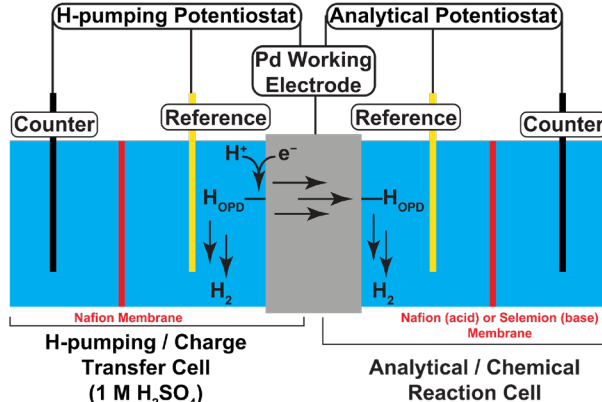
a



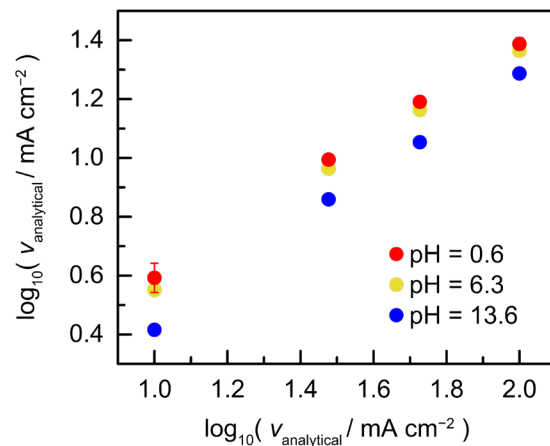
b



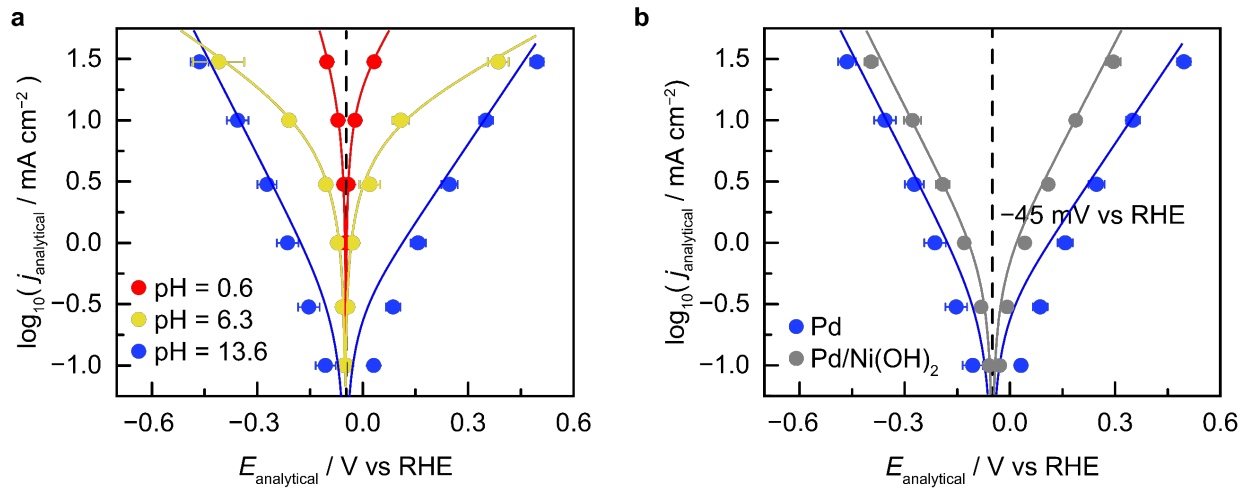
c



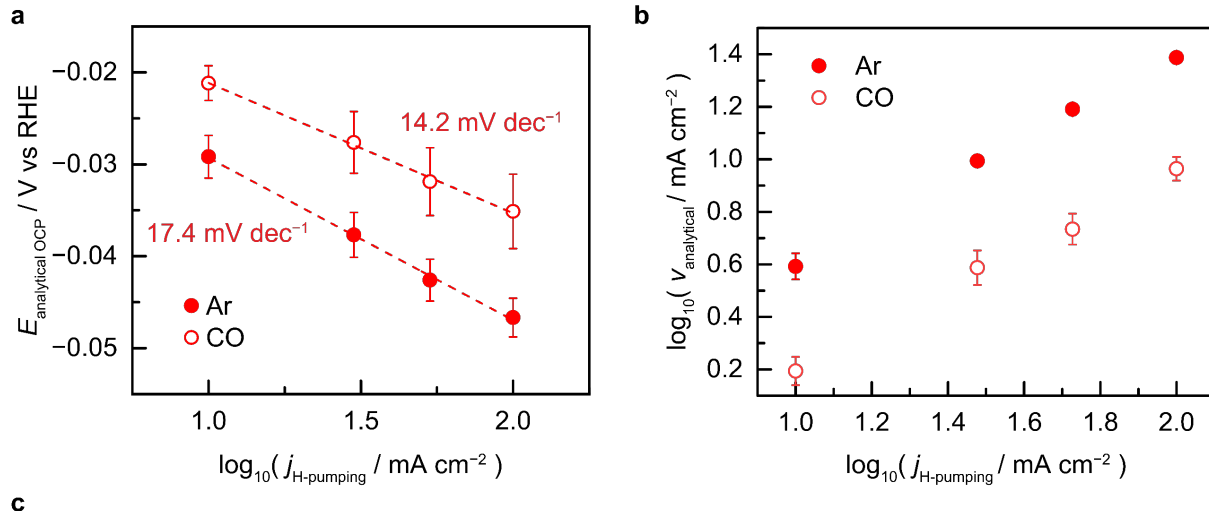
**S1.** Illustrations and photographs of the three different electrochemical double cell configurations (a) 2 compartment cell (b) 3 compartment cell and (c) 4 compartment cell.



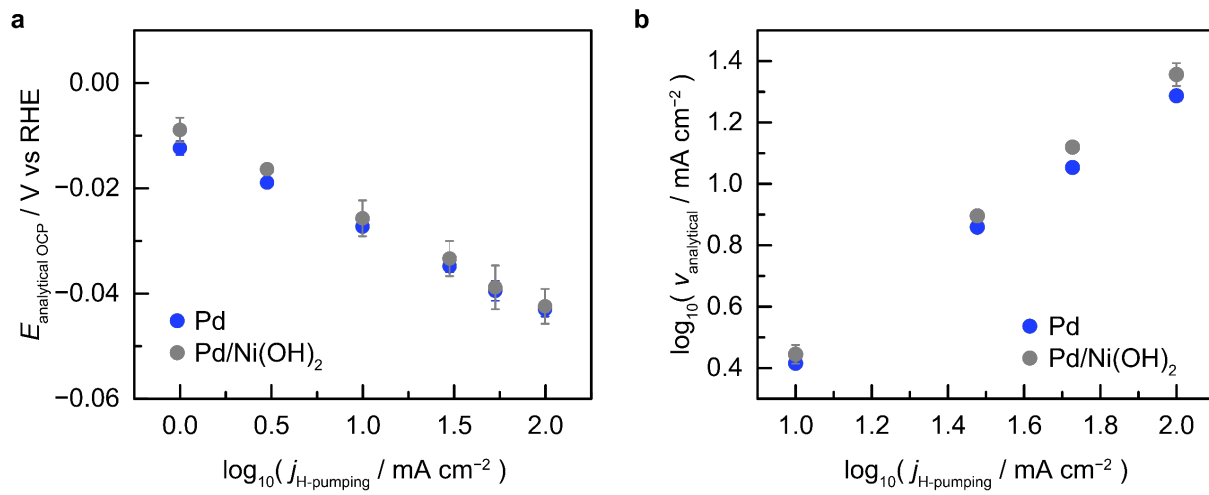
**S2.** Rate of H<sub>2</sub> release at the analytical interface ( $v_{H_2\text{An}}$ ) versus the total current passed at the H-pumping interface ( $j_{H\text{-P}}$ ) under different pH conditions including 13.6 (blue), 6.3 (yellow) and 0.6 (red). Error bars indicate standard deviations obtained from three or more replicates (some error bars are smaller than the data point markers).



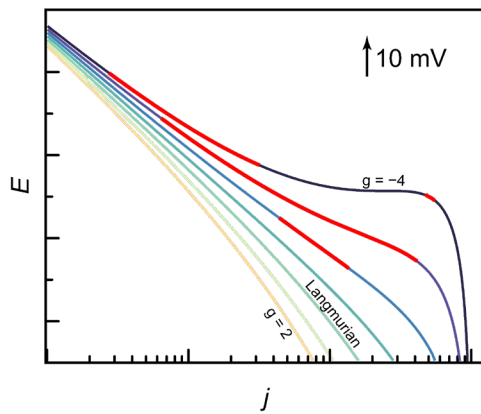
**S3.** Fitting the double polarization Butler-Volmer plots for (a) pH = 0.6 (red), pH = 6.3 (yellow) and pH = 13.6 (blue) and (b) pH = 13.6 on bare (blue) and Ni(OH)<sub>2</sub> decorated Pd (grey). Error bars indicate standard deviations obtained from three or more replicates (some error bars are smaller than the data point markers).



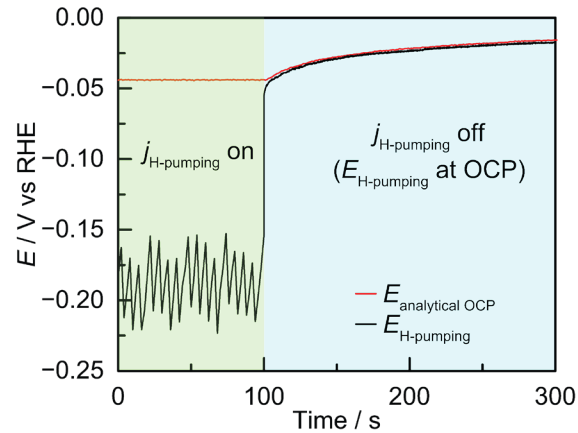
**S4.** CO poisoning effects on the Pd electrochemical double cell. **(a)** Open circuit potential dependence of the analytical interface ( $E_{\text{An OCP}}$ ) under Galvanostatic polarization at the H-pumping interface ( $j_{\text{H-p}}$ ), with (open red circles) and without (closed red circles) CO. **(b)** The rate of  $\text{H}_2$  evolution at the analytical interface ( $j_{\text{An}}$ ) versus the current density passed at the H-pumping interface ( $j_{\text{H-p}}$ ), with (open red circles) and without (closed red circles) CO. **(c)**  ${}^1\text{H}$  NMR spectra of the electrolyte pre- and post-electrolysis (blue and green, respectively), showing no detectable formic acid from electrolysis under CO.  ${}^1\text{H}$  NMR reference spectra of 0.1 M formic acid (dotted line). Error bars indicate standard deviations obtained from two or more replicates (some error bars are smaller than the data point markers).



**S5. (a)** Open circuit potential dependence of the analytical interface ( $E_{\text{An OCP}}$ ) under Galvanostatic polarization at the H-pumping interface ( $j_{\text{H-P}}$ ), with (blue) and without  $\text{Ni(OH)}_2$  (grey) in 1 M NaOH. **(b)** The rate of  $\text{H}_2$  evolution at the analytical interface ( $j_{\text{An}}$ ) versus the current passed at the H-pumping interface ( $j_{\text{H-P}}$ ), with (blue) and without  $\text{Ni(OH)}_2$  (grey) in 1 M NaOH. Error bars indicate standard deviations obtained from three or more replicates (some error bars are smaller than the data point markers).

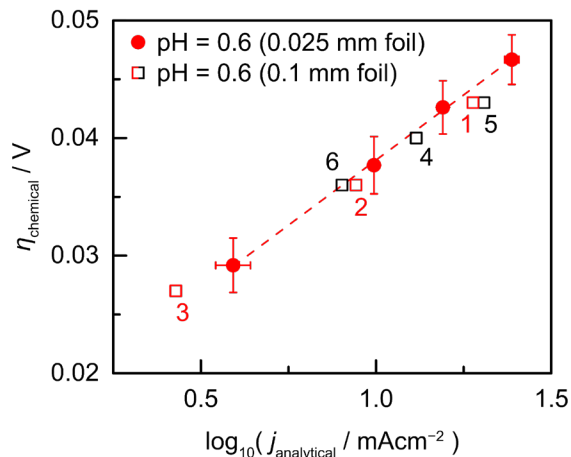


**S6.** Tafel plots of a Volmer-Tafel mechanism with a rate limiting Tafel reaction for a Langmuriian isotherm, and also Frumkin isotherms with both repulsive ( $g > 0$ ) and associative ( $g < 0$ ) interactions. The red regions denote where a  $20 \pm 5 \text{ mV dec}^{-1}$  Tafel slope would be observed.



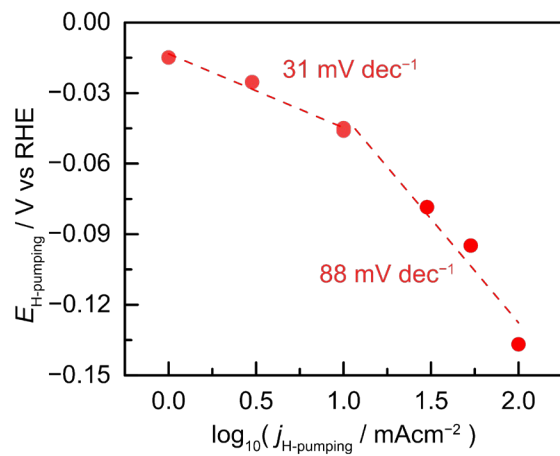
**S7.** Potential of both the H-pumping interface (black) and the analytical interface (red) under galvanostatic polarization of  $-100 \text{ mA cm}^{-2}$  at the H-pumping interface (green region) and immediately after polarization is turned off (blue region).

Upon termination of polarization, the OCP on both interfaces collapses to the same value (we observe a consistent offset of approximately 2 mV which we ascribe to a slight offset between reference electrodes). Furthermore, both OCP values decay towards more positive values together. Taken together, we believe that the minimal deviation in OCP between the H-pumping and analytical interface post electrolysis suggests that the chemical potential difference of surface H between the H-pumping and analytical interface is minimal, which would be consistent with a system that is not under diffusion limitations.



**S8.** The rate of H<sub>2</sub> release at the analytical interface ( $\nu_{\text{analytical}}$ ) versus the chemical overpotential at that interface ( $\eta_{\text{chemical}}$ ) for a 0.025 mm (red circles) and 0.1 mm thick Pd foil (red and black open squares). Error bars indicate standard deviations obtained from three or more replicates (some error bars are smaller than the data point markers). The 0.1 mm thick Pd foil experiment was performed only once via a staircase electrolysis program on the H-pumping interface. The numbers correspond to the sequence in which electrolysis conditions were applied. Potentials were measured with a Ag/AgCl reference electrode calibrated to the RHE.

The use of a thicker Pd foil results in a largely unchanged scaling of H<sub>2</sub> release at the analytical interface with  $\eta_{\text{chemical}}$  measured, suggesting that the influence of H diffusion through the Pd membrane has nominal effect on the interfacial surface H chemistry occurring at the analytical interface.



**S9.** Potential-current relationship observed at the H-pumping interface when the analytical interface is held at the open circuit potential. Potentials were measured with a Ag/AgCl reference electrode calibrated to the RHE.

## Supplementary References

1. Schreier, M., Yoon, Y., Jackson, M. N. & Surendranath, Y. Competition between H and CO for Active Sites Governs Copper-Mediated Electrosynthesis of Hydrocarbon Fuels. *Angew. Chem.* **130**, 10378–10382 (2018).